Monitoring the record-breaking wave event in Melilla harbour (SW Mediterranean Sea)

Pablo Lorente[1], Marta De Alfonso[1], Pilar Gil[1], Fernando Manzano[1], Anna Magdalena Matulka[1], Begoña Pérez-Gómez[1], Susana Pérez-Rubio[1] and M. Isabel Ruiz[1]

[1]Puertos del Estado, Madrid, 28042, Spain

Correspondence to: Pablo Lorente (plorente@puertos.es)

Abstract. ~~The accurate monitoring and understanding of violent weather-related hazards are decisive to adopt prevention strategies and enhance the socio-ecological resilience of coastal communities.~~ During the 4th-5th of April 2022, a~~A~~ record-breaking wave storm hit Melilla harbour (~~Alborán~~ SW Mediterranean Sea) with the violent overtopping of breakwaters. This unprecedented episode was compared against the six most extreme events previously registered by Melilla coastal buoy during 2011-2022 to disentangle their common atmospheric driving mechanisms. A ~~during the 4th-5th of April 2022. The maximum significant wave height (SWH) and mean period registered by a coastal buoy were 7.32 m and 9.42 s, respectively, beating previous historical records. Port decision-makers precautionary suspended maritime operations for security reasons due to the prevailing harsh weather, the overtopping of breakwaters and the presence of extreme harbour agitation (1.41 m) and sea level oscillations dominated by the infragravity band. In this work, the record-breaking event was analysed and retrospectively compared against six previous extreme wave episodes. All of them were connected with similar large-scale atmospheric driving forces: a~~ dipole-like sea level pressure (SLP) pattern, characterised by two adjacent (northwestern~~northern~~) high and (southeastern) low pressure systems, ~~which~~ induced ~~strong~~ intense easterly winds and high waves over the entire ~~Alborán Sea~~SW Mediterranean Sea. The 2022 record-breaking event differed from the rest in the much stronger SLP gradient (2 Pa·km^{-1}) and north-easterly winds (above 20 m·s^{-1}), which concurrently gave rise to a ~~-~~ maximum significant wave height (SWH$_o$) and mean period (T$_m$) of 7.32 m and 9.42 s, respectively, beating previous historical records. The associated return period decreased from 53 to 25 years, which must be considered for updated security protocols and sound design of future port facilities. Hourly observations from Melilla tide gauge covering the 2011-2022 period were used to investigate the relationship between offshore energetic waves penetrating into the harbour and the sea state inside. The harbour agitation, which also reached a record-breaking value (1.41 m) during the storm, was proved to be modulated by both the offshore SWH$_o$ (correlation coefficient of 0.87) and T$_m$. The highest values of agitation (above 1 m) were registered for incident high waves coming from the angular sector comprised between 50º and 70º (clockwise from true north) with T$_m$ and peak period (T$_p$) values above 7 s and 10 s, respectively. By contrast, the astronomical tide and the storm surge had negligible effects on harbour agitation during the seven extreme wave events. Infragravity waves, with periods between 30 s and 300 s and maximum values up to 0.58 m during the 2022 storm, were also detected within the harbour basins and exceeded previously reported peaks. The energy in the infragravity band (IGE) was significantly correlated (0.96) with an

Con formato: Superíndice
Con formato: Subíndice
Con formato: Subíndice
Con formato: Color de fuente: Automático
Con formato: Color de fuente: Automático
Con formato: Color de fuente: Automático
Con formato: Subíndice
Con formato: Subíndice
Con formato: Subíndice
Con formato: Subíndice

offshore forcing parameter proportional to $SWH_o^2 \cdot T_p$, evidencing that energetic swell was responsible for the highest IGE values (above 2000 $m^2 \cdot s$). ~~The common atmospheric configuration seems to predominantly feature during the same stage of the year, a 6-week period between late February and early April, contrasting with NW Spanish harbours where the storm season typically spans from November to March. Finally~~Furthermore, a 30-year (1993-2022) regional wave reanalysis ~~product~~ was used to characterise the intra-annual variability of the 99^{th} percentile ~~(P99)~~ of SWH_m ~~along~~ over the Alborán Sea at monthly timescale and identify the existence of trends. Results revealed that the intensity of extreme wave events impacting Melilla harbour and surrounding areas have increased for April while observed trends indicate a significant decrease of the ~~P~~99^{th} percentile of SWH_m for June and October. Finally, outcomes from this work could be useful to implement a multi-hazard early warning system and ad hoc mitigation plans within the harbour territory.

Con formato: Superíndice

Con formato: Superíndice

Con formato: Subíndice

Con formato: Superíndice

Con formato: Subíndice

1 Introduction

Over recent decades, climate change and extreme weather events have attracted growing public concern and political attention due to its widespread detrimental impact on the marine environment and human wellbeing (Konisky et al., 2015). While the global ocean is already experiencing anthropogenic-driven variations such as gradual warming, acidification, and sea level rise (IPCC, 2022), sustained pressure from climate change is even more significant on semi-enclosed basins like the Mediterranean Sea ~~due to its singular geomorphology~~ (Chiggiato et al., 2023; Juza and Tintoré, 2021) and also on exposed sectors like harbour systems (Verschuur et al., 2023; Izaguirre et al., 2021).~~.~~

The Mediterranean Sea has long been recognized as a vulnerable climate change hot spot (Tuel and Eltahir, 2020), seriously jeopardised by marine pollution episodes or litter accumulation (Soussi et al., 2020; Ramirez-Llodra et al., 2013). This region is often affected by marine heat waves, mass mortality events and violent hazards, ranging from storm surges and flash floods to rogue waves and Medicanes (Dayan et al., 2023; Clementi et al., 2022; Garrabou et al., 2022; Milglietta and Rotunno, 2019; Wolff et al., 2018; Cavaleri et al., 2012). Served as examples, the 2018 Medicane Zorbas or the 2020 S~~s~~torm Gloria ~~resulted~~ caused several~~in~~ casualties and multi-million damages in susceptible coastal areas (~~Álvarez-Fanjul et al., 2022; Scicchitano et al., 2021;~~ Lorente et al., 2021; ~~Sotillo et al., 2021;~~ De Alfonso et al., 2021; Pérez-Gómez et al., 2021; Sotillo et al., 2021; Scicchitano et al., 2021).

Consequently, there is an increasing awareness not only about the potential anthropogenic influence on the intensity of these extreme weather episodes (Eyring et al., 2021) but also about the unavoidable need of gaining deeper insight into the underlying physical processes~~, (Eyring et al., 2021) .~~ already identified as one of the World Climate Research Program's Grand Challenges (WCRP website). The~~ir~~ accurate monitoring of extreme events ~~comprehensive monitoring~~ is crucial to implement adaptation policies and~~,~~ adopt prevention strategies~~, reduce coastal vulnerability, and mitigate the destructive effects in human infrastructures and related services~~ that should eventually result in the enhancement of coastal communities' resilience (~~Izaguirre et al., 2021;~~ Linnenluecke et al., 2012). In response to this requisite, successive editions of the Copernicus Ocean State Report initiative have traditionally placed special emphasis on the multi-parameter analysis of severe sea states previously occurred in the Mediterranean basin ((Table 2). Álvarez-Fanjul et al., 2022; Clementi et al., 2022; Giesen et al., 2021; De Alfonso et al., 2020; Berta et al., 2020; Bensoussan et al., 2019; Notarstefano et al., 2019; Kokkini et al., 2018).

Recent initiatives like ECCLIPSE (assEssment of CLImate change in Ports of Southwest Europe) Interreg Sudoe project (ECCLIPSE website) have focused on analysing the impact of climate change on seaports. Although this topic has historically received less consideration than the corresponding impact for beach systems (Sánchez-Arcilla et al., 2016a and 2016b), the central role of ports in countries'' growth and globalised economy have motivated a plethora of newborn studies (Portillo Juan et al., 2022; Izaguirre et al., 2021), some of them devoted toin the Mediterranean Sea (Portillo Juan et al., 2022; Sierra et al., 2015 and 2017, Sánchez-Arcilla et al., 2016b). In this sense, one of the main objectives of ECCLIPSEthis project was to establish the fundamentals of a climate change observatory for Spanish ports, aiming at monitoring essential ocean variables and gaining an holistic understanding of extreme violent weather from its physical drivers to its impact on port operability and infrastructure (Table 3).. Climate-driven extreme coastal hazards have been acknowledged to impose heavy socio-economic tolls as port downtime leads to reduction of safety levels and wide trade losses due to the interruption of both the maritime transport and global supply-chain networks (Verschuur et al., 2022).

Following the footprints of ECCLIPSE, this is work attempts to characterise the record-breaking storm that hit the Alborán Sea (SWsouth-western Mediterranean Sea, Figure 1-a) with wave heightswaves above 7 m during the 4th-5th of April 2022 and evaluate the energetic response of Melilla harbour basins (Figure 1, b c) under the penetrating wave action. Port operations were precautionary disrupted due to the prevailing harsh weather conditions and , the violent overtopping of breakwaters and the presence of record harbour agitation and infragravity (IG) waves with periods between 25-30 s and 300-600 s (Bellafont, 2019; Elgar et al., 1992). breakwaters. While one ship was evacuated from its berth and later sheltered at the lee of Ras Taksefi Cape (Figure 1, b), structural damages were reported in the seawall tip and in several boats and marina pontoons.

Within this context, it is noteworthy that the Melilla area is usually dominated by a low energy wave climate with mean significant wave heights (SWH) below 0.7 m (Table 4), in contrast to other western Mediterranean Sea regions like the Gulf of Lion (Figure 1, a) where highly energetic waves (above 5 m) can be frequently observed during wintertime (Guizien, 2009). ThereforeA, a retrospective comparison of the present study case against six previous extreme wave events previously registered at Melilla coastal buoy (Figure 1b) during 2011-2022 (with SWH values above the 99.9th percentile, denoted in Figure 1-d) was conducted not only to put the former into a broader historical context but also to disentangle their common driving mechanisms (i.e., the predominant atmospheric conditions at synoptic scale).

The return period associated with these extreme wave episodes, which is defined as the average time interval between two consecutive events exceeding a specific wave height value, was also calculated. This concept is often used in marine engineering for the design of port facilities and the identification of dangerous events, providing a means for rational

Con formato: Fuente: (Predeterminada) Times New Roman, 10 pto, Color de fuente: Automático, Diseño: Claro

Con formato: Superíndice

Con formato: Superíndice

Con formato: Color de fuente: Rojo

Con formato: Color de fuente: Automático

Con formato: Color de fuente: Automático

Con formato: Color de fuente: Automático

decision making and risk assessment (Salvadori et al., 2013). For instance, harbour breakwaters are commonly designed to withstand 100-year return period metocean conditions without significant damage, while having service lifetimes of similar durations (Todd et al., 2012; Gutierrez-Serret et al., 2009).

Additionally, following the approach of Pérez-Gómez et al. (2021) for 2020 S~~s~~torm Gloria, high frequency (2 Hz) sea level data and agitation observations provided by Melilla tide-gauge (Figure 1~~,~~ b ~~c~~) during 2011-2022 were used to investigate the relationship between offshore energetic conditions and the sea state ~~inside~~ within~~of~~ the harbour~~r (including the IG energy band).~~. Precise estimations of agitation (i.e., oscillations within the port due to wind waves) are essential for downtime analysis and efficient port management (Romano-Moreno et al., 2022). Equally, ~~The monitoring of~~ infragravity (IG) waves with periods between 30 s and 300 s (Bellafont, 2019; Elgar et al., 1992; Munk, 1950) were examined since ~~IG waves is a red-hot issue since~~ their presence in semi-closed ports of small to intermediate size (where the surface water area and depth are about 1-10 km^2 and 5-10 m, respectively) may cause excessive ship motions at berth and unacceptable forces on mooring lines and fenders that could result in~~, among other problematic effects~~ ship collisions and significant damage to vessels and port facilities (Costas et al., 2022; Bellotti and Franco, 2011). Under adverse circumstances, IG waves can be highly amplified by the basin geometry due to resonant processes (commonly referred to as seiches), resulting in large water level fluctuations and strong horizontal currents ~~within the harbour~~ that disturb port operations (unsafe and inefficient cargo activities) and negatively impact on cost-time efficiency (López and Iglesias, 2014; Okihiro et al., 1993)~~, as reflected in Table 3~~.

Finally, a 30-year (1993-2022) regional wave reanalysis product developed in the frame of the Copernicus Marine Service for the Mediterranean Sea was analysed to~~: i) infer its accuracy in the study area and thereby the historical occurrence of similar extreme episodes; ii)~~ characterise the spatio-~~spatial~~ temporal variability of the long-term extreme ~~value~~ wave climate along the Alborán Sea ~~along the Alborán Sea~~. The intra-annual variability of the 99th percentile (~~the 99th percentile (~~P99 hereinafter)~~)~~ for the~~of~~ significant wave height ~~SWH~~ was examined over this subregion at monthly timescale to identify potential trends, thereby complementing similar studies previously focused on the intra-seasonal (Barbariol el al., 2021) or the inter-annual (Zacharioudaki et al., 2022b; Morales-Márquez et al., 2020) climate variability of extreme waves in the entire Mediterranean basin.

This work is structured as follows: Section 2 outlines the observational and modelled data sources. Section 3 describes the methodology adopted. Results are presented and discussed in Section 4. Finally, principal conclusions are drawn in Section 5.

2 Data

All the observational and modelled ~~products~~ datasets used in this study are ~~gathered in Table 1 and~~ briefly described below. Complementary information about them is gathered in Table 1 and Table 2.

Con formato: Color de fuente: Automático

Con formato: Superíndice

Con formato: Fuente: Sin Negrita

2.1 In situ observational data

Although the two in situ instruments used in this work were deployed before 2009, the time span for the observational datasets was standardized to 2011-2022 for consistency reasons as the collection of directional wave data started on April 2010 (Table 2).

2.1.1 Melilla coastal buoy

A Datawell scalar buoy was moored at 15 m depth in April 2008, close to Melilla harbour (Figure 1b). It was replaced in April 2010 by a Triaxys buoy able to provide directional information. This in situ device, operated by Puertos del Estado, collects hourly-averaged estimations of diverse wave parameters (product ref. no. 1 in Table 1), encompassing the significant wave height (SWH_o), maximum wave height (MWH_o), mean period (T_m), peak period (T_p) and incoming mean wave direction (MWD_o). The quality control applied to data time series, defined by the Copernicus Marine In situ Team (Copernicus Marine In situ Team, 2017), consisted of a battery of automatic checks performed to flag and filter inconsistent values. For the Mediterranean Sea, the spike test was based on the difference between sequential measurements of SWH_o, T_m, and T_p so they were discarded, respectively, when the difference exceeded 3 m, 4 s and 10 s. Occasional gaps (not larger than 6 h) were linearly interpolated to ensure the continuity of the records.

2.1.2 Melilla port tide-gauge

A radar tide-gauge, manufactured by Miros and operated by Puertos del Estado as part of its REDMAR network (Pérez-Gómez et al., 2008 and 2014), was deployed inside of Melilla harbour in October 2007 (Figure 1b). Quality-controlled 2 Hz sea level data (product ref. no. 2 in Table 1) contain information of sea level oscillations with periods above 1 s, capturing all sea surface height variability including waves, high-frequency sea level oscillations (HFSLO) and tides. Sea level oscillations with periods over 1 h were extracted using a 10th-order Chebyshev low-pass filter with a cut frequency of 1/3600, whereas wave agitation (with periods below 30 s) was obtained using an 8th-order Butterworth high-pass digital filter with a cut frequency of 1/30. HFSLO (with periods between 30 s and 1 h) were obtained by subtracting the two previous time series from the raw 2 Hz data signal. Then, a simplified four band energy spectrum was also calculated to facilitate the understanding of the energy distribution in the HFSLO band: i) period between 30 s and 5 min (IG waves); ii) period between 5 min and 15 min; iii) period between 15 min and 30 min; iv) period between 30 min and 1 hour. For further details about the frequency-domain analysis (used to describe how energy is distributed among all frequencies and to determine the most energetic frequency in an hourly basis) and time-domain analysis (used to determine the hourly amplitudes of the HFSLO: maximum -$HFSLO_{max}$- and average of the highest third heights -$HFSLO_{13}$-), the reader is referred to as García-Valdecasas et al. (2021). Finally, 20-minute estimations of $HFSLO_{max}$, $HFSLO_{13}$, IG wave energy (IGE) and agitation were subsampled at hourly intervals (Table 2) and examined to assess the impact of extreme wave storms inside the harbour. Likewise, hourly estimations of total water fluctuations, astronomical tides and storm surge component were qualitatively

Con formato: Normal
Con formato: Subíndice
Con formato: Subíndice
Con formato: Subíndice
Con formato: Fuente: (Predeterminada) Times New Roman, Color de fuente: Automático
Con formato: Fuente: (Predeterminada) Times New Roman, Color de fuente: Automático
Con formato: Fuente: (Predeterminada) Times New Roman, Color de fuente: Automático
Con formato: Fuente: (Predeterminada) Times New Roman, Color de fuente: Automático
Con formato: Fuente: (Predeterminada) Times New Roman, Color de fuente: Automático
Con formato: Fuente: (Predeterminada) Times New Roman, Color de fuente: Automático
Con formato: Fuente: (Predeterminada) Times New Roman, Color de fuente: Automático
Con formato: Fuente: (Predeterminada) Times New Roman, Color de fuente: Automático
Con formato: Fuente: (Predeterminada) Times New Roman, Color de fuente: Automático
Con formato: Fuente: (Predeterminada) Times New Roman, Color de fuente: Automático
Con formato: Fuente: (Predeterminada) Times New Roman, Color de fuente: Automático
Con formato: Fuente: (Predeterminada) Times New Roman, Color de fuente: Automático
Con formato: Título 3
Con formato ...
Con formato ...
Con formato: Superíndice
Con formato: Superíndice
Con formato ...
Con formato ...
Con formato ...
Con formato ...
Con formato ...
Con formato ...
Con formato ...
Con formato ...
Con formato: Subíndice
Con formato: Subíndice

analysed to infer any potential sea level rise that could take place simultaneously (or in close sequence) to the extreme wave storms.

Con formato: Fuente: (Predeterminada) Times New Roman, Color de fuente: Automático

2.2 Modelled data

The time span for the modelled datasets was standardized to 1993-2022 for consistency reasons (Table 2).

Con formato: Título 3

2.2.1~~1~~ ERA5 reanalysis

ERA5 reanalysis (product ref. no. 3 in Table 1), ~~is the fifth-generation reanalysis for the global climate and weather~~which is generated by the European Centre for Medium-Range Weather Forecast (ECMWF), ~~. Data is available from 1940 onwards (product ref. no. 1 in Table 1). ERA5~~ provides hourly estimates from 1940 onwards for a large number of atmospheric and oceanic parameters ~~(among other quantities)~~ which are regridded, respectively, to a 0.25° and 0.5° regular grid. In this work, hourly maps of modelled sea level pressure (SLP), ~~and~~ wind at 10 m height (W10) and significant wave height (SWH_m) were analysed at ~~synoptic~~ synoptic scale (19ºW-5ºE, 26ºN-56ºN) for the 1993-2022 period (Table 2) in order to disentangle the common atmospheric configurations that drove the most extreme wave events registered by Melilla buoy.~~.~~

Con formato: Subíndice

~~**2.2 Wave forecast model**~~

~~**Puertos del Estado and the Spanish Meteorological Agency run twice a day a WAM-based wave forecast system (product ref. no. 2 in Table 1), providing hourly wave outputs with a 72-h forecast horizon. In this work, hourly maps of SWH were used to examine the fingerprint of the wave storm during the 4th of April 2022 (Figure 1, a-b).**~~

~~**2.3 Tide-gauge**~~

~~**A radar tide-gauge, manufactured by Miros and operated by Puertos del Estado as part of its REDMAR network (Pérez-Gómez et al., 2008), was deployed inside of Melilla harbour in October 2007 (Figure 1, b-c). Since it provides quality-controlled high frequency (2 Hz) sea level data (product ref. no. 3 in Table 1), immediate evaluation of specific physical phenomena contained in raw data (such as meteotsunamis and IG waves) can be achieved (García-Valdecasas et al., 2021). Furthermore, 20-minute averaged estimations of agitation (i.e., oscillations within the port due to wind waves) were examined for the period 2015-2022 to assess the impact of the wave storm.**~~

~~**2.4 In situ coastal buoy**~~

~~**A Datawell scalar buoy was moored at 15 m depth in April 2008, close to Melilla harbour (Figure 1, b-c). Two years later, it was replaced by a Triaxys buoy able to provide directional information. This in situ device, operated by Puertos del Estado, collects quality-controlled hourly estimations of sea surface temperature and diverse wave parameters (product ref. no. 4 in Table 1).**~~

2.2.2~~5~~ Multi-year wave product

The multi-year wave product of the Mediterranean Sea Waves forecasting system (product ref. no. 4~~5~~ in Table 1) is based on a~~the~~ WAM model suite that predicts hourly wave parameters at 1/24° horizontal grid resolution. The atmospheric wind forcing used in WAM model consists of hourly 0.25° horizontal resolution ERA5 reanalysis from the ECMWF. The multi-year product consists of ~~and contains~~ a reanalysis dataset (MED reanalysis hereinafter), which spans from 1 January 1993 to 31 December 2022, ~~(from January 1993)~~ and an interim dataset covering the period after the reanalysis until one month before present. ~~The dataset is composed of hourly wave parameters at 1/24° horizontal resolution.~~ In the present work, only the MED reanalysis was used: hourly SWH$_m$ estimations ~~over the entire Alborán Sea (Figure 1, a)~~ were ~~analysed~~ examined for the selected ~~the~~ 30-year period ~~1993-2022~~ (Table 2) to characterise the spatio-temporal variability of the long-term extreme wave climate affecting the Alborán Sea, in general, and specifically Melilla harbour area. Equally, hourly maps of propagation direction (MWD$_m$) were depicted to assess the prevalent wave directionality during the extreme events.

3 Methodology

As not all extreme metocean hazards necessarily have destructive impacts on coastal areas, there is not a worldwide consensus on the protocol for their categorization. ~~A weather-related event is generally defined as extreme when a single or several interconnected variables persistently exceed specific thresholds, which can be determined according to percentile-based values, fixed absolute values or return periods~~ (Radovic and Iglesias, 2018).

Con formato: Título 3

Con formato: Subíndice

Con formato: Subíndice

In th~~e present~~is work, ~~we firstly used~~ the 99.9th percentile (P99.9 hereinafter)~~method, which~~ of SWH_o for the 12-year time series (2011-2022) provided by Melilla coastal buoy was used ~~defines extreme events as the occurrence of values higher than the reference~~as ~~P99~~ threshold ~~for a certain number of hours. P99 values, along with P50, P90 and P99.9 values, were computed on the whole time series (2008-2022) of diverse wave parameters registered by Melilla coastal buoy in order to comprehensively characterise the wave climate Melilla area (Table 4) and~~to ~~categorise~~ select and tag chronologically a manageable number of ~~seven~~ extreme wave events previously occurred. Once shortlisted, these episodes were characterized in terms of intensity (magnitude of diverse wave parameters) and duration (hours above the P99 of SWH_o), placing the focus on the joint occurrence of interconnected extremes that might exacerbate the coastal impact compared to individual hazards occurring in isolation. Complementarily, hourly maps of SWH_m were depicted to explore if the extreme wave events shared similar synoptic features in terms of severity and spatial distribution.

In order to elucidate the potential existence of common driving mechanism, the predominant atmospheric conditions (in terms of SLP and W10) at synoptic scale that led to the record-breaking storm were retrospectively compared to those giving rise to previous extreme wave events. Additionally, the temporal distribution of extreme episodes affecting Melilla area was derived from the 12-year observational time series of SWH_o and T_m to elucidate if they showed a relevant preference for a specific stage of the year. The annual cycle was split into six evenly spaced 50-day intervals and a longer 65-day summertime interval that did not negatively impact on the consistency of the percentages of occurrence obtained as extreme wave events during summer remained marginal regardless of the interval length selected.

T~~Complementarily, t~~he return period associated with th~~os~~ese extreme wave episodes was derived from~~calculated. The notion of return period, which is defined as the average time interval between two consecutive events exceeding a specific SWH value, is often used in marine engineering for the design of port facilities and the identification of dangerous events, providing a means for rational decision making and risk assessment (Salvadori et al., 2013). For instance, harbour breakwaters are commonly designed to withstand 100-year return period metocean conditions without significant damage, while having service lifetimes of similar durations (Todd et al., 2012; Gutierrez-Serret et al., 2009). In this work, the analysis was conducted using~~ hourly~~the~~ time series of SWH_o ~~SWH~~ for two different periods: ~~: a) 20~~2011~~10~~-202~~0~~1 (~~(~~before the record-breaking storm) ~~)~~ and ~~(b) 20~~2011~~10~~-2022 (~~(~~including the storm). To this purpose, we assumed:~~.~~

i) an exceedance threshold based on the 95th percentile (P95) value of the dataset following the approach proposed by Harley (2017) and Fanti et al. (2023) for coastal storm analysis.

ii) 5-day distance between two independent storms. Although there is some subjectivity in how a time series is partitioned into separate storms, the broadly accepted criteria states that the independence between consecutive events is achieved by imposing that storm peaks must be separated by a time period longer than 3 days, which is the average lifetime of extra-tropical cyclones (Trigo et al. 1999). For instance, the most intense activity period of Storm Gloria in the western Mediterranean Sea ranged between 20 and 23 January 2020 (Amores et al., 2020; Lorente et al., 2021). Since adjacent peaks separated by 5 days will correspond to waves generated from different low-pressure systems, meteorologically

- **Con formato:** Superíndice
- **Con formato:** Subíndice
- **Con formato:** Subíndice
- **Con formato:** Fuente: 10 pto, Color de fuente: Automático, Diseño: Claro
- **Con formato:** Fuente: 10 pto, Color de fuente: Automático, Diseño: Claro
- **Con formato:** Subíndice
- **Con formato:** Color de fuente: Automático
- **Con formato:** Color de fuente: Automático
- **Con formato:** Color de fuente: Automático
- **Con formato:** Color de fuente: Rojo
- **Con formato:** Subíndice
- **Con formato:** Subíndice
- **Con formato:** Color de fuente: Automático
- **Con formato:** Color de fuente: Automático
- **Con formato:** Párrafo de lista;Bullet List Paragraph;Lettre d'introduction;Numbered paragraph 1;Paragrafo elenco;1st level - Bullet List Paragraph;Heading 4 bullet;Paragrafo elenco numerato;Bullet point;Enumeración 2;Bullet Paragraph;List Paragraph1, Sangría: Izquierda: 0 cm, Sangría francesa: 0,75 cm, Numerado + Nivel: 1 + Estilo de numeración: i, ii, iii, … + Iniciar en: 1 + Alineación: Izquierda + Alineación: 0,63 cm + Sangría: 1,9 cm
- **Con formato:** Color de fuente: Automático
- **Con formato:** Color de fuente: Automático
- **Con formato:** Sangría: Izquierda: 0 cm, Sangría francesa: 0,75 cm
- **Con formato:** Color de fuente: Automático
- **Con formato:** Color de fuente: Automático

independent events were identified by applying a moving time window of 5 days length between consecutive storms, in accordance to Mackay and Johanning (2018a and 2018b).

The long-term extreme sea state was characterised by using the Peak over Threshold (POT) method (Goda, 19~~9~~88) with the fitting of a t~~T~~hree-Parameter Weibull probability distribution to the SWH_o ~~SWH~~ observations. The POT method is based on extracting, from the recorded time series, those individual storms which surpass the aforementioned exceedance threshold of SWH_o in the peak of the storm and are not dependant upon another one due to their proximity in time~~, and that surpass the exceedance threshold of SWH (established for each region in function of its own wave climate, see Table 5) in the peak of the storm~~. The three~~3~~-parameter Weibull distribution was computed following the approach proposed by De Alfonso et al. (2021) to obtain the return period for the maximum SWH_o ~~SWH~~ registered during the ~~seven~~ selected extreme wave events ~~(Table 5)~~.

~~In situ data time series were processed as follows: spikes or spurious values were discarded, and occasional gaps were linearly interpolated to ensure the continuity of the records. The statistical metrics used in the present study to compare two data sets x = {x₁, x₂, x₃ … x_N} and y = {y₁, y₂, y₃ … y_N} (where 1, 2, … N represent the time steps) include the mean, the standard deviation, and the correlation coefficient, defined respectively as:~~

~~$$\bar{x} = \frac{1}{N}\sum_{i=1}^{N} x_i \qquad (1)$$~~

~~$\sigma = \sqrt{}$ [redacted] (2)~~

~~$$\text{Correlation} = \frac{1}{N-1}\sum_{i=1}^{N}\left(\frac{x_i-\bar{x}}{\sigma_x}\right)\left(\frac{y_i-\bar{y}}{\sigma_y}\right) \qquad (3)$$~~

~~where σ_x and σ_y are the standard deviation of x and y, respectively.~~

Furthermore, t~~T~~he relationship between ~~energetic~~ offshore sea states~~conditions and agitation~~ and IG waves within Melilla harbour ~~maximum height inside the harbour (IG_{max})~~ was investigated. Here we focused on its most common type: those induced by the non-linear interactions between incident wind short waves (Belloti and Franco, 2011). While IG waves tend to go unnoticed to human perception in deep waters (heights of the order of few cm), they can abruptly increase near the coastline and even exceed 1 m (Aucan and Ardhuin, 2013), contributing significantly to nearshore processes (beach erosion) and affecting coastal structures (Okihiro et al. 1993). Significant efforts have been previously devoted to analysing the connection between offshore wave parameters and IGE, either at the shore (in the form of run-up) or in the nearshore area (surf zone). While Guza and Thornton (1982) found that the IG component of wave run-up increased linearly with increasing offshore SWH_o. Stockdon et al. (2006) concluded that the IG component scaled better with $SWH_o \cdot L$ (where L represents the deep-water wavelength) and was actually independent of the foreshore slope. In the same line, Senechal et al. (2011) reported that IG wave run-up during extreme storm conditions was significantly less scatter when correlated with $SWH_o \cdot L$ than with SWH_o only. By contrast, Inch et al. (2017) reported that nearshore IG waves were best predicted using an offshore

Con formato: Color de fuente: Automático
Con formato: Color de fuente: Automático
Con formato: Color de fuente: Rojo
Con formato: Resaltar
Con formato: Sangría: Primera línea: 0 cm
Con formato: Color de fuente: Automático
Con formato: Color de fuente: Automático
Con formato: Color de fuente: Automático
Con formato: Subíndice
Con formato: Color de fuente: Automático
Con formato: Color de fuente: Automático
Con formato: Color de fuente: Automático
Con formato: Color de fuente: Automático
Con formato: Color de fuente: Automático
Con formato: Color de fuente: Automático
Con formato: Fuente: (Predeterminada) Times New Roman, Color de fuente: Automático
Con formato: Color de fuente: Automático
Con formato: Color de fuente: Automático
Con formato: Color de fuente: Automático
Con formato: Color de fuente: Automático

forcing parameter that is proportional to $SWH_o^2 \cdot T_p$. These contradictory findings reveal that further research on the subject is required and suggest that nearshore IGE is unlikely a function of any single environmental factor (Lashley et al., 2020).

While the four aforementioned field studies focused on low-to-mild-sloping sandy beaches, the present work attempts to relate IGE measured within a harbour with offshore wave parameters. To this aim, a rough approximation approach (based on three simplifications) was adopted:

i) local slope effects were not included, similarity to Stockdon et al. (2006).

ii) IGE registered at Melilla tide gauge was scaled with SWH_o^2, $SWH_o \cdot L$ and $SWH_o^2 \cdot T_p$ despite the fact that IGE is affected by wave–structure interaction processes (diffraction and reflection, to name the main ones) which are not so relevant in open sandy beaches.

iii) Although Melilla coastal buoy is moored at 15 m depth (d), the deep-water approximation is broadly accepted since the relative depth (defined as d/L) is above 0.5 the 78% of the time during 2011-2022 (not shown). Therefore, the wavelength can be defined as $L=(g \cdot T_m^2)/2\pi$, where the gravity acceleration g is 9.8 $m \cdot s^{-2}$. As a consequence, we can derive from point ii) that IGE was scaled with SWH_o^2, $SWH_o \cdot T_m^2$ and $SWH_o^2 \cdot T_p$.

~~The spectra of 2 Hz sea level oscillations measured by the tide gauge revealed a high energy content in the IG band during the seven storms, reaching a record value during the E7 event. As the IG energy in the nearshore has been documented to be positively correlated with offshore SWH (Inch et al., 2017; Stockdon et al., 2006), a scatter plot was computed to disentangle which peak periods could yield severe IG waves within the port. Furthermore~~Additionally, ~~the high frequency (30 s – 1 h)~~ HFSLO~~sea level oscillations~~ (with periods between 30 s and 1 h)~~heights~~ and harbour agitation (with periods below 30 s) data recorded by ~~within~~ Melilla tide-gauge during 2011-2022 were thoroughly examined. On one hand, HFSLO heights ~~harbour~~ observed during the s~~even~~elected extreme ~~storms~~ events were categorized based on specific IG wave thresholds ~~(Table 6)~~ which are universally common to all locations (McComb et al., 2020; McComb, 2011). This approach is valid since spectra of the 2 Hz data (not shown), generated to identify energetic sea level variability inside the port, were dominated by energy in the IG band during these storms. On the other hand, total seawater levels were examined to disentangle if they exerted a relevant role in the sharp increase of harbour agitation during the extreme wave events and if astronomical tides were thereby enhanced by storm surge effects. In this context, connected extremes are of particular concern for harbour operability, as their individual effects may interact synergistically and cause more damage in port structures than isolated extreme events (Velpuri et al., 2023).

Finally, potential long-term changes in the extreme sea state climate during the 30-year period analysed (1993-2022) were assessed over the Alborán Sea. As a preliminary step, the accuracy of MED reanalysis was evaluated at the grid point 2.916ºW-35.354ºN (denoted with a green rectangle in Figure 1b) closest to Melilla coastal buoy and located at a distance of 3450 m. Concurrent estimations of hourly SWH_o and SWH_m were compared for the period 2011-2022 and the best linear fit of scatter plot was computed. The statistical metrics used in the present study to compare two data sets included the mean, the standard deviation, and the Pearson correlation coefficient (Emery and Thompson, 2001). Afterwards,

Con formato: Color de fuente: Automático
Con formato: Color de fuente: Automático
Con formato: Color de fuente: Automático
Con formato: Color de fuente: Automático
Con formato: Color de fuente: Automático
Con formato: Color de fuente: Automático
Con formato: Color de fuente: Automático
Con formato: Color de fuente: Automático
Con formato: Color de fuente: Automático
Con formato: Color de fuente: Automático
Con formato: Párrafo de lista;Bullet List Paragraph;Lettre d'introduction;Numbered paragraph 1;Paragrafo elenco;1st level - Bullet List Paragraph;Heading 4 bullet;Paragrafo elenco numerato;Bullet point;Enumeración 2;Bullet Paragraph;List Paragraph1, Sangría: Izquierda: 0 cm, Sangría francesa: 0,5 cm, Numerado + Nivel: 1 + Estilo de numeración: i, ii, iii, … + Iniciar en: 1 + Alineación: Izquierda + Alineación: 0,63 cm + Sangría: 1,9 cm
Con formato: Color de fuente: Automático
Con formato: Color de fuente: Automático
Con formato: Superíndice
Con formato: Color de fuente: Automático, Sin Superíndice / Subíndice
Con formato: Color de fuente: Automático
Con formato ...
Con formato: Color de fuente: Automático
Con formato: Color de fuente: Automático
Con formato: Color de fuente: Automático
Con formato: Color de fuente: Automático
Con formato: Color de fuente: Automático
Con formato: Sin Resaltar
Con formato: Subíndice
Con formato: Superíndice
Con formato: Superíndice
Con formato: Superíndice
Con formato: Color de fuente: Rojo
Con formato ...
Con formato ...
Con formato ...
Con formato: Color de fuente: Automático
Con formato: Subíndice
Con formato: Subíndice

Equally, the connection between harbour agitation and the wave field (SWH, period and incoming direction) outside the port was investigated through the computation of a scatterplot, assuming the following relationship (Inch et al., 2017):

$$\text{Agitation} \sim \sqrt{\ } \qquad (4)$$

The deep-water wavelength (L) is defined as follows:

$$L = \frac{g \cdot T^2}{2\pi} \qquad (5)$$

where the gravity acceleration g is 9.8 m·s-2 and T is the wave period in seconds, respectively.

Finally, potential long-term changes in the extreme sea state climate during the 30-year period analysed (1993-2022) were assessed through the estimation of maps of linear trend for the P99 of SWH_m SWH over the entire Alborán Seas were obtained over the entire Alborán Sea at monthly timescales. The attention was particularly focused on the intra-annual variability in order to complement prior research dealing with intra-seasonal and inter-annual variability of extreme waves in the entire Mediterranean basin. (Amarouche et al., 2022a; Barbariol el al., 2021; Zacharioudaki et al., 2022b; Morales-Márquez et al., 2020). The presence of temporal tendencies trends in the P99 of SWH_m SWH reanalysis time series was evaluated with two well-known non-parametric tests, which have been recently documented as the most used for trend detection in the Mediterranean Sea (De Leo et al., 2023):.

i) i) trends were calculated using the Sen´s slope estimator of P99 because it is not subject to the influence of extreme values (outliers) and therefore is more consistent than simple linear regression methods (Sen, 1968). Although P95 is also commonly used (Fanti et al., 2023), P99 was selected as reference percentile for the most extreme wave events affecting Melilla area, in agreement with previous approaches reported in the literature (Zacharioudaki et al., 2022b, Barbariol et al., 2021).

i)

ii) ii) the statistical significance at the 90% confidence interval was assessed at each grid point with the Mann-Kendall test (Mann, 1945; Kendall, 1962), in accordance with similar works previously published (Caloiero and Aristodemo, 2021; Barbariol et. aAl, 2021). Afterwards, a specific subdomain (2.70ºW-3.00ºW, 35.02ºN- 35.48ºN) in the vicinity of Melilla harbour was selected and the statistical significance was spatially-averaged to infer if this area is affected by meaningful trends.

4 Results

4.1 Extreme events analysis

The P99.9 of SWH_o (set to 4.45 m and derived from the 12-year time series provided by Melilla coastal buoy) was used as threshold to detect the most extreme wave events (Figure 1c). Seven storms were identified and tagged chronologically from

Con formato: Sangría: Primera línea: 0 cm

Con formato: Sangría: Primera línea: 1,27 cm

Con formato: Fuente: 10 pto

Con formato: Inglés (Reino Unido)

Con formato: Inglés (Reino Unido)

Con formato: Inglés (Reino Unido)

Con formato: Sangría: Izquierda: 0 cm, Sangría francesa: 0,5 cm

Con formato: Fuente: Sin Negrita, Color de fuente: Automático

Con formato: Párrafo de lista;Bullet List Paragraph;Lettre d'introduction;Numbered paragraph 1;Paragrafo elenco;1st level - Bullet List Paragraph;Heading 4 bullet;Paragrafo elenco numerato;Bullet point;Enumeración 2;Bullet Paragraph;List Paragraph1, Sangría: Izquierda: 0 cm, Sangría francesa: 0,5 cm, Numerado + Nivel: 1 + Estilo de numeración: i, ii, iii, … + Iniciar en: 1 + Alineación: Izquierda + Alineación: 0,63 cm + Sangría: 1,9 cm

Con formato: Fuente: Sin Negrita, Color de fuente: Automático

E1 to E7. They presented values ranging from 5.05 m (E3) to 7.32 m (E7), as shown in Table 3. The associated T_m values, which ranged from 6.83 (E2) to 9.42 s (E7), surpassed the P99 (set to 6.25 s, Figure 1d). The seven episodes also showed concurrent high values of MWH_o and T_p, emerging in the ranges 6.83-12.11 m and 9.13-10.75 s (Table 3). The unprecedented storm that hit Melilla harbour during the 4th-5th of April 2022 (E7) clearly exhibited unprecedentedbeat historical records of values for each wave parameter: SWH in terms of intensity and duration. The P99, set to 2.92 m (Table 4) and derived from a long-term time series provided by a Melilla coastal buoy (Figure 1, b-c), was abruptly exceeded during 42 consecutive hours. Tthe peak of SWH_o SWH (7.32 m) was, coincident with the greatesta values maximum value of MWH_o (12.11 m) and mean $T_{m\text{wave period}}$ (9.42 s),, jointly beatbeating all previous historical records (Figure 1, c-d). Additionally, a retrospective comparison of the record-breaking storm against the six most extreme events previously occurred in Melilla was performed to put the former into a broader historical context. The seven episodes were tagged in chronological order, as shown in Figure 1d. All of them exhibited SWH values fairly above the P99.9 of SWH (4.44 m, Table 4) and above the P99 of mean period (6.29 s, Table 4). In terms of storm duration (Table 3), defined as the number of consecutive hours above the P99 of SWH_o (set to 3.01 m), E1 and E6 were significantly shorter (<20 h) than long-lasting E2 and E4 events (>50 h). The duration of E3 and E5 (27-31 h) events can be considered similar to E7 (37 h). From a directional perspective (Figure 1, f), the prevailing incoming wave directions during the 2011-202212 year period 2011-2022 were NE (41%) and NE-E (43%), with an overall associated mean value of (58º ± 37)º (Figure 1e). These are the most common origins for waves recorded at Melilla coastal buoy due to its particular emplacement, sheltered to the east of Ras Taksefi Cape (Figure 1, b). As a result, the shadow effect of this coastal promontory prevents the angular spreading of the storms coming from the westernmost sector. For extreme wave events with SWH_o above P99 (3.01 m), the predominant incoming wave direction was NE-E with a 72% of occurrence, whereas the remaining 28% corresponded to the NE sector (Figure 1f).

Hourly maps of SWH_m for E1-E6 events (Annex 1) and E7 (Figure 1a) shared common synoptic features such as the peak of SWH_m (above 4.5 m) over the entire Alborán Sea. A secondary peak could be found over the Gulf of Cádiz for E1, E2, E4, E5 and E7 episodes, while E3 barely showed it. In the case of E6 event, the peak of SWH_m over the easternmost part of the Alborán Sea was not so high (around 4 m) but affected broader areas of the SW Mediterranean Sea. The spatial patterns of SWH_m and MWD_m, zoomed in the surrounding areas of Melilla harbour (small maps exposed in the lower right corner of each panel of Annex 1) revealed a similar visual resemblance for SWH_m and a uniform MWD_m field from the NE. The record-breaking E7 event stood out from the rest due to the severity of the storm, with SWH_m above 5.5 m over the entire Alborán Sea (Figure 1a) but also in the vicinity of Melilla harbour (Figure 1b).

4.2 Return period analysis

The analysis was conducted using hourly time series of SWH from Melilla coastal buoy for two different periods, assuming an exceedance threshold of 2 m (previously derived from the wave climate in the study area) and 5 days distance between two independent stormy events (Table 5). For the period 202011 10-20210, the entire hourly time series of SWH_o was fitted

Con formato: Subíndice
Con formato: Subíndice
Con formato: Superíndice
Con formato: Superíndice
Con formato: Fuente: Sin Negrita
Con formato: Subíndice
Con formato: Subíndice
Con formato: Fuente: (Predeterminada) Times New Roman, Color de fuente: Automático
Con formato: Fuente: (Predeterminada) Times New Roman, Color de fuente: Automático
Con formato: Subíndice
Con formato: Color de fuente: Automático
Con formato: Color de fuente: Automático
Con formato: Color de fuente: Automático
Con formato: Color de fuente: Automático
Con formato: Color de fuente: Automático
Con formato: Color de fuente: Automático
Con formato: Color de fuente: Automático
Con formato: Subíndice
Con formato: Color de fuente: Automático
Con formato: Color de fuente: Automático
Con formato: Color de fuente: Automático
Con formato: Color de fuente: Automático
Con formato: Subíndice
Con formato: Subíndice

to a three~~3~~-parameter Weibull distribution, leading to return periods of 3.25-4.51 years for the extreme wave events E1 to E6 (Table 4). Notwithstanding, the E7 event was associated with a 53~~45~~-year return period which highlights the extraordinary magnitude of this twice-in-a-century high-impact episode.

For the period ~~20~~2011~~10~~-2022, which already included ~~not only the E6 event (March 2021) but also~~ the record-breaking E7 storm (April 2022), a new fitting of the three~~3~~-parameter Weibull probability distribution to the SWH_o ~~SWH~~ observations was performed and the associated Weibull parameters (threshold, scale and shape) were updated (Table 4~~5~~). Results revealed that the return period related to E1 to E6 events decreased by 17~~20~~-224% to 2.69~~5~~-3.51 years, while the updated E7 return period dropped by 53~~45~~%~~-~~ from 53 years to ~~(~~25 years~~)~~. These relevant outcomes should be applicable in the design and construction of new facilities at Melilla harbour and also integrated into the port operations planning and day-to-day logistics activities.

4.3 Driving atmospheric conditions

The prevailing atmospheric conditions at synoptic scale during the seven extreme wave storms were inferred from the ERA5 reanalysis of SLP and W~~wind at~~ 10~~-m height~~. The SLP ~~pattern~~ map for E7 event (Figure 2a) exhibited ~~was characterised~~the so-called hybrid Rex block (Sousa et al., 2021; Lupo, 2021; Rex, 1950), a large-scale blocking pattern characterized by two adjacent (northwestern) high and (southeastern) low pressure systems~~by two adjacent (north-western) high and (southern) low pressure systems (Figure 2, a)~~. This type of blocking is usual during the transition phase from an Omega block (midlatitude high-pressure centre surrounded by two low pressure systems on its western and eastern flanks) to a pure Rex shape (a north–south dipole pattern of SLP). Blocking episodes in Europe have been long acknowledged as persistent atmospheric disturbances that can lead to weather extremes (Kautz et al., 2022). As a consequence, t~~T~~his ~~persistent~~ dipole was visible for the whole investigation period, whereas it followed a clockwise rotation. The derived pressure gradient (above 2 Pa·km^{-1}) gave rise to very strong north-easterly winds (above 20 m·s^{-1}) that affected broad areas of the SW Mediterranean and Alborán Seas, while extremely intense easterlies were channelled through the Strait of Gibraltar due to its specific geometric configuration (Figure 2~~,~~ b). In the Gulf of Cádiz (denoted in Figure 1a), the wind field exhibited a counterclockwise rotation around the low-pressure core.

The analyses of the six previous extreme events ~~(listed in Figure 1d)~~ revealed that all of them shared very similar meteorological conditions: i) a northwestern-southeastern ~~dipole-like~~ hybrid Rex pattern of SLP anomalies (Annex ~~1~~2), in contrast to the climatological mean (Figure 2~~,~~ c) that shows two well-known semi-permanent pressure systems (i.e., the Azores High at middle latitudes and the Icelandic Low at subpolar latitudes); ii) a peak of wind speed (> 15 m·s^{-1}) over the entire Alborán Sea, where easterlies blew ~~persistently~~ strongly along both sides of the Strait of Gibraltar (Annex 3~~2~~). Only the event E6 showed a slightly different structure (Annex 3~~2,~~ f), with moderately strong winds (13-15 m·s^{-1}) blowing from the NE and massively ~~only~~ affecting the entire western~~NW~~ Mediterranean Sea. In terms of persistence, intense winds steadily affected the study area for 1-2.5 days, except in the case of E1 and E6 events where the duration was shorter (14-16 h), as derived indirectly from the time that the SWH_o consecutively exceeded the P99 (Table 3).

Con formato: Fuente: (Predeterminada) Times New Roman, 10 pto, Color de fuente: Automático
Con formato: Fuente: (Predeterminada) Times New Roman, 10 pto, Color de fuente: Automático
Con formato: Fuente: (Predeterminada) Times New Roman, 10 pto, Color de fuente: Automático
Con formato: Fuente: (Predeterminada) Times New Roman, 10 pto, Color de fuente: Automático
Con formato: Fuente: (Predeterminada) Times New Roman, 10 pto, Color de fuente: Automático
Con formato: Fuente: (Predeterminada) Times New Roman, 10 pto, Color de fuente: Automático
Con formato: Fuente: (Predeterminada) Times New Roman, 10 pto, Color de fuente: Automático
Con formato: Fuente: (Predeterminada) Times New Roman, Color de fuente: Automático
Con formato: Fuente: (Predeterminada) Times New Roman, 10 pto, Color de fuente: Automático
Con formato: Fuente: (Predeterminada) Times New Roman, Color de fuente: Automático
Con formato: Fuente: (Predeterminada) Times New Roman, Color de fuente: Automático
Con formato: Fuente: (Predeterminada) Times New Roman, Color de fuente: Automático
Con formato: Superíndice
Con formato: Superíndice
Con formato: Color de fuente: Automático
Con formato: Subíndice
Con formato: Color de fuente: Automático
Con formato: Color de fuente: Automático

The primary factors that jointly triggered the record-breaking E7 wave storm were the short distance (1400 km) between the two main pressure systems along with the relatively deep (below 1000 hPa) system of low pressures over the Gulf of Cádiz (Figure 2a). The resulting SLP gradient was anomalously powerful (above 2 Pa·km^{-1}), leading to very strong easterlies (up to 20 m·s^{-1}, as shown in Figure 2b) that ultimately induced high (~6 m) waves over the entire Alborán Sea (Figure 1a). The previous six episodes also presented intense (albeit 25-50% weaker) SLP gradients, ranging from 1.01 Pa·km^{-1} (E4, Annex 2d) to 1.48 Pa·km^{-1} (E6, Annex 2f), due to the usually longer distances (ranging from 1900 km to 3000 km) comprised between both pressure systems (Annex 2). Although the E1 event exhibited SLP cores with similar separation (1438 km, showed in Annex 2a), the low-pressure system was not so deep (1016 hPa), in contrast to the E7 event where minimum SLP values dropped below 1000 hPa (Figure 2a).

FurthermoreFinally, it should be noted that the seven extreme episodes took place during the same stage of the year, a 506-dayweek period between late February and early April (Figure 2d and Table 3Figure 1, d). Therefore, it might be deduced that the large-scale atmospheric configuration blocks leading to severe sea states (above the P99 of SWH$_o$ and T$_m$) in Melilla apparently tend to be more probable during the winter-to-spring transition period, in agreement. with previous blocking climatologies for the eastern North Atlantic (Kautz et al., 2022; Barriopedro et al., 2006). The primary factor that triggered the record-breaking wave storm (E7 event) was the short distance (1400 km) between the two main pressure systems, rather than the associated SLP values (Figure 2, a-b). The resulting SLP gradient was anomalously powerful (above 2 Pa·km^{-1}), leading to very strong, persistent easterlies that ultimately induced high waves over the entire Alborán Sea. The P99 of SWH, set to 2.92 m (Table 4) and derived from long-term time series provided by Melilla coastal buoy (Figure 1, b-c), was abruptly exceeded during 42 consecutive hours (Figure 1, d). The previous six episodes also presented intense (albeit weaker) SLP gradients, ranging from 1.01 Pa·km^{-1} (event E4, Annex 1d) to 1.48 Pa·km^{-1} (event E6, Annex 1f), due to the usually longer distances (ranging from 1900 km to 3000 km) comprised between both pressure systems (Annex 1). Although the E1 event exhibited SLP cores with similar separation (1438 km, showed in Annex 1a), the low-pressure system was not deep (1016 hPa), in contrast to the E7 event where minimum SLP values dropped below 1000 hPa (Figure 2, a).

4.4 Sea state within the port

An accurate estimation of the historical harbour wave agitation is fundamental for many practical applications such as port downtime analysis (Romano-Moreno et al., 2022). The analysis of hourly time series of agitation provided by Melilla tide gauge revealed that there was a record-breaking value during E7 event (1.41 m, Figure 2e), while the six previous events also exceeded the P99.9 threshold (0.56 m, Figure 3a). The agitation response is usually determined by wave penetration into the harbour arising from the combination of diverse parameters: SWH$_o$, T$_m$, MWD$_o$, astronomical tide and storm surge outside the port (Camus et al., 2018). As shown in Figure 2e and Annex 4, the impact of the last two elements on harbour agitation during the seven extreme events was negligible due to a number of factors, namely: i) Melilla harbour waters are

Con formato: Subíndice
Con formato: Sin Superíndice / Subíndice
Con formato: Color de fuente: Automático
Con formato: Color de fuente: Automático
Con formato: Color de fuente: Automático
Con formato: Color de fuente: Rojo
Con formato: Subíndice
Con formato: Subíndice

characterized by a maximum tidal range of 0.40 m; ii) for each extreme event, the evolution of harbour agitation was independent from the tidal phase as the peak of agitation was not coincident with high tides; iii) during E7, the low-pressure core (~1000 hPa) was located in the Gulf of Cadiz (western side of the Strait of Gibraltar, Figure 2a) so the storm surge affecting Melilla harbour was small (~5 cm, Figure 2e); iv) during the previous six extreme events (E1-E6), the meteorological residual was even negative (Annex 4), ranging from -2 cm (E3) to -14 cm (E2).

Hourly scatter plots evidenced the strong relationship between the agitation inside the port and the wave conditions outside the port registered by Melilla coastal buoy (Figure 3, b-d). The best linear fit of scatter plot between the agitation and SWH_o revealed a significantly high correlation coefficient (0.87). During the 12-year period analysed (2011-2022), there were 967 hourly agitation values above the P99 threshold (0.36 m): the 89% of them were associated with waves coming from the predominant sector comprised between 50º and 70º (clockwise from true north), while 6% of them were related to incoming waves with angles emerging from 70º to 90º (Figure 3b). The remaining 5% was assigned to waves with an angular spread ranging from 30º to 50º. Therefore, the overall agitation is direction-dependent due to the harbour orientation (Figure 1b) and its inherent structural design (mouth width, port layout configuration, etc.). Additionally, harbour agitation was also importantly modulated by offshore period, as shown in Figure 3 (c-d). Agitation values above the P99 were generally observed when T_m and T_p values were above 4 s and 6 s, respectively. Equally, the highest values of agitation (above 1 m height) were associated with T_m and T_p values above 7 s and 10 s, respectively. It seems reasonable to deduce that the record-breaking harbour agitation (1.41 m) registered during E7 event was caused by the combined effect of unprecedented values of SWH_o (7.32 m), MWH_o (12.11 m) and T_m (9.42 s) in tandem with a very high value of T_p (10.75 s) and a MWD_o (55º) comprised within the predominant angular sector (50º-70º) previously mentioned.

Operational thresholds in the IG band, which are common to all locations, have been historically proposed for safe conditions during port operations (McComb et al., 2020; McComb, 2011). Since the spectra of 2 Hz sea level oscillations measured inside the harbour by Melilla tide gauge (not shown) revealed a high energy content in the IG band during the seven storms, $HFSLO_{13}$ values registered during the seven extreme events (which contained not only the predominant contribution of oscillations in the IG band but also of oscillations with periods between 5 min-1 hour) were categorized according to this methodology (Figure 3e). The exploration of hourly timeseries of $HFSLO_{13}$ showed that E1 and E6 events surpassed 0.15 m threshold (denoted as "extreme caution" in Figure 3e), while the remaining five events exceeded also the "danger" threshold (0.20 m), with an unprecedented value of 0.31 m during the E7 episode. Likewise, hourly values of $HFSLO_{max}$ went clearly beyond 0.35 m during the extreme episodes, reaching the record-breaking value of 0.58 m during E7 event. Furthermore, IGE was scaled with SWH_o^2, $SWH_o \cdot T_m^2$ and $SWH_o^2 \cdot T_p$ (Figure 3, f-h). ~~Here we focus on the most common type of IG waves, those induced by the non-linear interactions between incident wind short waves (Belloti and Franco, 2011). While IG waves tend to go unnoticed to human perception in deep waters (heights of the order of few cm), they can abruptly increase near the coastline and even exceed 1 m (Aucan and Ardhuin, 2013), contributing significantly to nearshore processes (beach erosion) and affecting coastal structures (Okihiro et al. 1993).~~

Con formato: Subíndice
Con formato: Subíndice
Con formato: Subíndice
Con formato: Subíndice
Con formato: Subíndice
Con formato: Subíndice
Con formato: Subíndice
Con formato: Subíndice
Con formato: Subíndice

The hourly timeseries of maximum sea level oscillations heights (30 s – 1 h) showed that the seven extreme episodes surpassed the P99 (0.28 m) threshold, while only four of them -E3, E4, E5 and E7- exceeded also the P99.9 (0.44 m) threshold (Figure 3, a). According to the spectra content of 2 Hz data, these oscillations are highly dominated by the IG band energy during the analysed events. The spectra of 2 Hz sea level oscillations measured by the tide gauge revealed a high energy content in the IG band during the seven storms, reaching a record value during the E7 event.

Operational thresholds in the IG band, which are common to all locations, have been historically proposed for safe conditions during port operations (McComb et al., 2020; McComb, 2011). According to Table 6, hourly records of sea level oscillations (30 s – 1 h) height for the seven extreme events (not shown) were beyond the limit of 0.2 m, except for E6 case where values ranged from 0.047 to 0.194 m. The maximum height values were clearly above that limit, with an unprecedented value of 0.58 m during the E7 episode.

The best linear fit of each scatter plot showed very high correlationsa strong correlation (0.8): 0.94, 0.93 and 0.96, respectively. Therefore, IGE was best predicted using an offshore forcing parameter that is proportional to $SWH_o^2 \cdot T_p$, in accordance with Inch et al. (2017). between the offshore incident SWH and the energy in the IG band inside the port (Figure 3, b). As expected, the highest IGE energy values (above 1500 $m^2 \cdot s$) wereas observed for energetic swell waves (with SWH_o SWH and T_p peak period above 5 m and 1010 s, respectively).

An accurate estimation of the historical harbour wave agitation is fundamental for many practical applications such as port downtime analysis (Romano-Moreno et al., 2022). The analysis of 20-m timeseries of agitation provided by Melilla tide gauge revealed that the seven extreme events exceeded the P99 (0.38 m) threshold and only E6 did not beat the P99.9 (0.6 m) threshold (Figure 3, c). In particular, during E7 event there was a record-breaking value of agitation (1.4 m), a 233% higher than the P99.9 threshold. The agitation response is determined by wave penetration into the harbour arising from the combination of diverse parameters, namely: SWH, wave period and direction, astronomical tide and storm surge outside the port (Camus et al., 2018). The impact of the last two elements on harbour agitation was not taken into account since: i) the Mediterranean Sea is a microtidal environment with tidal ranges below 1 m (Samper et al., 2022); and ii) the low-pressure core was located in the western side of the Strait of Gibraltar so the storm surge affecting Melilla harbour was negligible (Figure 2, a). An hourly scatter plot evidenced the strong linear relationship between the agitation inside the port and the wave conditions outside the port registered by Melilla coastal buoy (Figure 3, d), with a significant correlation coefficient of 0.92 for an 8-year period (2015-2022). For the 655 hourly agitation values above the P99 threshold, the 90% were associated with waves coming from the predominant sector comprised between 50º and 70º (clockwise from true north), while 6% of them were related to incoming waves with angles emerging from 70º to 90º. The remaining 4% was assigned to waves with an angular spread ranging from 30º to 50º. The overall agitation is direction-dependent due to the harbour orientation (Figure 1, c) and its inherent structural design (mouth width, port layout configuration, etc.).

Con formato: Tachado

Con formato: Subíndice

4.5 Trends in extreme wave climate

The evolution on the extreme wave conditions over the Alborán Sea during the 30-year period analysed (1993-2022) was assessed. As a preliminary step, SWH_m estimation from a validation of the MEDregional wave reanalysis products wereas conducted compared against hourly in situ SWH_o estimations observations provided by Melilla coastal buoy (Figure 1, b-c) during the concurrent ,1214-year period (20201109-2022). To this aim, the MED reanalysis grid point (2.916ºW, 35.354ºN) closest to the moored buoy (located at a distance of 3450 m) was selected and both time series of SWH were compared. A significantly high correlation coefficient (0.965) for a set of 86925 77100 hourly data was derived from the best linear fit of scatter plot (Annex 5a3, a). Equally, the slope and intercept values were close to 1 (0.85) and moderately low (0.15), respectively.

Time series of annual P99 of SWH showed a consistent qualitative agreement between the reanalysis and buoy estimations (Annex 3, b). The quantitative differences emerged in the range from 0.01 m (2009) to 0.66 m (2015), with the reanalysis systematically underestimating extreme SWH conditions. The monthly P99 values of SWH for 2009-2022 exhibited a similar visual resemblance (red and blue lines in Annex 3c), with three dominant regimes: i) a 6-month calm period (from May to October), where P99 is below 2.5 m; ii) a shorter transitional season (from November to January) with an increasing P99 usually in the range 2.5-3 m; iii) a stormy period (from February to April) with monthly P99 above 4 m (3 m) for buoy (reanalysis) estimations. It should be noted that, for both datasets, the maximum P99 is detected for April. If the entire temporal reanalysis coverage 1993-2022 is considered, slight differences can be found in the monthly P99 (green line in Annex 3c): there is a drop of P99 for April and a noticeable increase of P99 for June and October. Such changes in the intra-annual variability of the extreme wave climate in Melilla will be further discussed soon afterwards.

These results revealed that MEDthe regional wave reanalysis, albeit accurate in Melilla region, seems to underestimate wave SWH_o heights, especially for extreme waves. Such systematic underestimation has been previously reported for the entire domain (Fanti et al., 2023; Zacharioudaki et al., 2022b) since shallow water processes cannot be properly captured by global and regional reanalysis because: i) the coastline and the bottom topography are not well resolved as the grid mesh is too coarse; ii) fetch limitations; iii) inherent uncertainties in the wind field used to force the wave model. These limitations are even more pronounced in regions with complex coastal configurations (sheltered by islands, headlands, and reefs) and in port-approach areas where sharp topo-bathymetric gradients pose special difficulties for accurate local predictions (Sánchez-Arcilla et al., 2016a). Nevertheless, according to Zacharioudaki et al. (2022b), the reanalysis skill can be considered robust and good enough to conduct further investigations about the wave climate affecting Melilla area and the related intra-annual variability in the Alborán Sea.

Thus, the yearly-averaged monthly P50 and P99 of SWH_m SWH were computed over the entire Alborán Sea for the 1993-2022 period (Annex 5, b-e4). In particular, we selected only March April and July as representative months of the stormy and calm seasons (peak of green line in Annex 3c) and calm period (minimum value), respectively. According to homogeneous spatial patterns of P50, the mean wave climate is rather similar for March April and July, only differing in the

Con formato: Subíndice

Con formato: Subíndice

Con formato: Color de fuente: Automático

Con formato: Color de fuente: Automático

magnitude: while March April is characterised by a P50 slightly above 1.1 m over Alborán open waters (Annex 5b) in March, P50 is around 0.7-0.8 in July (Annex 54, a cb). By contrast, significant differences can be found in the most energetic sea states (Annex 54, de-ed). In MarchApril, the P99 values around Melilla are up to 3 m, while they clearly exceedreach 4 m offshore (Annex 54, de). Peaks of 4.35 m are attained in the easternmost sub-basin, probably as a consequence of strong easterly winds. On the contrary, during July the largest P99 barely reaches 3 m in the central part of Alborán Sea, while the spatial distribution of P99 generally remains uniformly below 2 m in the rest of the spatial domain, including littoral areas and nearby regions of Melilla harbour (Annex 54, de).

The climate variability over the Alborán Sea was assessed by analysing the intra-annual variations in the extreme SWH_m wave conditions (Figure 4). Monthly trend maps of P99 of SWH were calculated for the period 1993-2022, revealing statistically significant changes in the vicinity of Melilla harbour for few specific months: while an increase of 2 cem·year^{-1} wais observed for April (Figure 4, a), a downward P99 trend of 1.5-2- cem·year^{-1} wais detected for June (Figure 4b, c) and October (Figure 4, cg) and, to a less extent, in July (Figure 4, e). The temporal trends for each month (Figure 4, d-fb,d,f,h), computed over the subdomain surrounding Melilla harbour (black box in Figure 4, a-c), visually supported visually the previous statement: t. While the trends were statistically significant at the 90% confidence interval for April, June, and October., in the case of July the observed downward trend was only significant at the 80% confidence interval.

By contrast, during both the second part of summer (August July--September) and the transitional season (November - February), monthly maps of P99 trends (not shown) did not exhibit statistically significant values over the entire Alborán Sea (Annex 5). Although The ttrend maps of P99 for March and March (Annex 5, c) and May (not shown) showed(Annex 5, d) showed, large areas with relevant positive trends and negative trends, respectively, but delimited over the easternmost part (2ºW-1ºW) of the Alborán basin.

s, they were spatially delimited to specific locations far away from Melilla harbour and the surrounding area (the scope of the present study) and therefore will not be further commented.

The long-term changes detected in the extreme wave climate over Melilla are, to a certain extent, comparable to those previously exposed by Barbariol et al. (2021). Although the wave reanalysis used and its associated temporal coverage (1980-2019) were different, this previous work reported both an upward trend for theof P99 of SWH_m SWH (about 0.8-1.2 cem·yeardecade^{-1}) and a non-significant trend in the vicinity of Melilla harbour for the extended winter (defined as NDJFM) and for summer (defined as JJA), respectively.. From a broader perspective focused on the entire western Mediterranean Sea, Barbariol et al. (2021) also documented a relevant positive trend (1.2 cm·year^{-1}) during winter in the Gulf of Lyon (denoted in Figure 1a) due to strong north-westerly Mistral winds. By contrast, Amarouche et al. (2022b) examined a 41-year (1979-2020) hindcast database and determined that the west coast of Gulf of Lyon was affected by a significant upward trend for all seasons, with a considerable annual increase (4 cm·year^{-1}) of maximum values of SWH_m. Complementarily, Amarouche et al. (2022a) demonstrated significant decadal increases in wave storm intensity and duration not only over the eastern part of the Alborán Sea but also in the Balearic basin. All these findings highlighted both the existence of an inter-seasonal variability of P99 of SWH_m and the importance of multi-temporal scales analysis.

Con formato: Color de fuente: Automático
Con formato: Color de fuente: Automático
Con formato: Color de fuente: Automático
Con formato: Color de fuente: Automático
Con formato: Color de fuente: Automático
Con formato: Color de fuente: Automático
Con formato: Color de fuente: Automático
Con formato: Color de fuente: Automático
Con formato: Color de fuente: Automático
Con formato: Color de fuente: Rojo, Español (España)
Con formato: Superíndice
Con formato: Subíndice
Con formato: Color de fuente: Automático
Con formato: Color de fuente: Automático
Con formato: Color de fuente: Automático
Con formato: Color de fuente: Automático, Subíndice
Con formato: Color de fuente: Automático
Con formato: Color de fuente: Rojo

5 Conclusions

Gaining a deeper, holistic understanding of extreme weather events and the related driving mechanisms has been identified as one of the World Climate Research Program's Grand Challenges (WCRP website) due to its detrimental impact on ecosystems health and societal assets (Hochman et al., 2022). Concerning the latter, climate-driven extreme coastal hazards have been long recognized to impose heavy socio-economic tolls, particularly aggravated in vulnerable semi-enclosed regions like the Mediterranean Sea and in exposed sectors like harbour systems (Verschuur et al., 2023).

As port downtime leads to reduction of safety levels and wide trade losses through maritime transport and global supply-chain networks (Verschuur et al., 2022), the accurate monitoring of violent weather-related episodes is decisive to adopt prevention strategies (i.e., wise design of safe port infrastructures) and mitigation measures that should eventually result in the enhancement of coastal communities' resilience.

In the present work, the attention is focused on the unprecedentedrecord-breaking storm that hit Melilla harbour (Alborán Sea, Figure 1ain the south-western Mediterranean Sea) during the 4th-5th of April 2022 with heavy rainfall and, strong easterly winds, which induced, and extremely high waves (above 7 m) with associated long mean periods (above 9 s) that simultaneously beat previous historical records (Figure 1, c-d). Tduring the 4th-5th of April 2022 (Figure 1, a). The P99 of SWH, set to 2.92 m and derived from hourly time series provided by a nearby coastal buoy (Figure 1, b-c), was abruptly exceeded during 42 consecutive hours. The maximum SWH and mean wave period registered were 7.32 m and 9.42 s, respectively, beating previous historical records (Figure 1, d-e). From a directional perspective, the prevailing incoming wave direction was the NE (Figure 1).

The long-term extreme wave distribution was characterised by using the return period and the percentile's method. The return period associated with different SWH values was calculated for two periods (2010-2020 and 2010-2022), revealing that it significantly decreased for the most extreme events (SWH above 5 m), as reflected in Table 5. In the specific case of the record-breaking E7 event, the return period (associated with this extreme wave event a SWH around 7.32 m) decreased from 5345 years to 25 years. These outcomes are essential for the safe design of future facilities at Melilla port (Naseef et al., 2019). Conversely, it is worth pointing out that the port is also subjected to a constant geometric modification (in the docks, basins, bathymetry, breakwaters, etc.) which in turn can induce additional variations in the port response to extreme wave events that should be further assessed.

The analysis of hourly time series of SWH, (2011-2022) revealed that there were seven episodes that exceededWith regards to the percentile's method, the P99.9 threshold (4.45 m), denoted chronologically from E1 to E7 in was applied as a threshold to the long-term time series of SWH (2008-2022) in order to categorise seven extreme wave events (Figure 1c, d). The retrospective comparison of the record-breaking E7 event against six previous extreme wave episodes (E1 to E6) revealed that all of them were connected with similar large-scale atmospheric driving blocksforces: -a dipole-like SLP pattern, characterised by two adjacent (northwestern) high and (southeastern) low pressure systems, induced strong easterly winds channelled over the entire Alborán Sea (Figure 2 a-b, Annex 21 and Annex 32). Furthermore, this common

Con formato: Subíndice

Con formato: Color de fuente: Automático

Con formato: Color de fuente: Automático

Con formato: Color de fuente: Automático

atmospheric configuration seems to predominantly feature during the same stage of the year, a 5~~06-~~day~~week~~ period between late February and early April (Figure 2d~~1, d~~). These findings contrast with other Spanish harbours (i.e., NW Iberian Peninsula) where the storm season typically spans from November to March (Ribeiro et al., 2023), highlighting the strong need of conducting a tailored assessment for each specific port and oceanographic region. Therefore, it might be deduced that large-scale atmospheric blocks leading to severe sea states in Melilla tend to be more probable during the winter-to-spring transition period. This outcome is in line with prior blocking climatologies for the eastern North Atlantic (Kautz et al., 2022; Barriopedro et al., 2006). In this context, previous works have also explored the dynamical links between blocking patterns and the Nort Atlantic Oscillation (NAO), which is the leading mode of atmospheric circulation variability over the Euro-Atlantic sector and is characterized by a seesaw of atmospheric mass between the Iceland Low and the Azores High (e.g., Hurrell and Deser 2009). The NAO appeared as the leading variability pattern during winter, accounting for the 45% of the blocking frequency variance (Barriopedro et al., 2006).

~~Long-term observations of~~H~~ h~~igh frequency (2 Hz) sea level and agitation observations during the 2011-2022 period, provided by Melilla tide gauge, were used to investigate the relationship between offshore energetic waves and the sea state inside of the harbour (Figure 3). A record-breaking value of harbour agitation (1.41 m)~~, a 233% higher than P99.9,~~ was recorded during the E7 event (Figure 3~~, c~~a). T~~Equally, t~~he highest agitation records (above 1 m) were registered for incident high waves coming predominantly from the sector comprised between 50º and 70º (clockwise from true north)~~,~~ with T_m and T_p values above 7 s and 10 s, respectively (~~as shown in~~ Figure 3, b-d).~~d.~~ Extreme sea level oscillations (30 s -1 h), which also reached record heights (up to 0.58 m), were linked to the highest values in the IG energy band ~~since the beginning of measurements~~ (Figure 3e~~, a~~). The seven extreme events in the Alborán Sea led to harsh sea conditions within the port: the energy in the IG band was significantly correlated (0.96~~8~~) with an offshore parameter proportional to~~the~~ SWH$_p$~~,~~T_p^2 ~~and peak periods recorded by the costal buoy~~, with energetic swell being responsible for the highest energies (above 2000 m^2·s), as shown in ~~(~~Figure 3 ~~(,~~ f-h~~b~~). Therefore, the IG waves related to energetic swell commonly observed in the NW Iberian coast, can also be present during extreme wave events in the Mediterranean coast, as previously reported for the 2020 S~~s~~torm Gloria by Pérez-Gómez et al. (2021) and Álvarez-Fanjul et al. (2022). ~~Equally, the highest agitation records were registered for incident high waves coming predominantly from the sector comprised between 50º and 70º (clockwise from true north), as shown in Figure 3d.~~

Additionally, MED~~a regional wave~~ reanalysis ~~product~~ was used to characterise the long-term mean (Annex 5~~4~~) and extreme (Figure 4 ~~and Annex 5~~) wave climate over the Alborán Sea for the period 1993-2022. The intra-annual variability of the P99 of SWH$_m$ was examined at monthly timescale to identify the existence of potential trends. Results seem to suggest that the intensity of extreme wave events impacting Melilla harbour has increased for April (Figure 4~~,~~ a and 4 ~~b~~d), while observed trends indicate a significant decrease of P99 for the SWH$_m$ during June (Figure 4b~~, e~~ and 4e ~~d~~) or October (Figure 4c~~, g-h~~ and 4f). Such alterations of outer-harbour wave climate conditions might impact on in-port wave agitation response as the amount of energy penetrating into the harbour would be different, as previously indicated by Sierra et al. (2015).

Con formato: Color de fuente: Automático

Con formato: Color de fuente: Automático

Con formato: Color de fuente: Rojo

Con formato: Subíndice

Con formato: Sin Superíndice / Subíndice

Con formato: Superíndice

Con formato: Superíndice

Con formato: Subíndice

Con formato: Subíndice

Still, it should be noted that the present work does not focus on the duration of extreme wave events over the SW Mediterranean Sea, so future endeavours should address this relevant aspect to complement the results here presented. ~~Equally~~Moreover, long-term historical changes in wave period and directionality are receiving increasing attention and should be further analysed to assess their specific impact on harbours operability (Erikson et al., 2022; Casas-Prat and Sierra, 2012). Permanent modifications in the wave direction might result in enhanced wave penetration into the harbour and thereby larger agitation as port protective structures were originally designed to dampen wind and short waves coming from a predetermined sector (Casas-Prat and Sierra, 2012). ~~-~~Likewise, offshore wave period also plays a primary role in the modulation of harbour agitation, as derived from Figure 3 (c-d). As a consequence, any sharp increase in both wave period and SWH$_{o}$ could lead to severe sea states within the port.

Regardless of the reported limitations of global and regional reanalyses (inherent to their coarse spatial resolution) when used at coastal and port scales (Fanti et al., 2023; Zacharioudaki et al., 2022b), the MED~~wave~~ reanalysis used in this work can be considered a robust first-guess estimator for the present intra-annual variability assessment of extreme waves in Melilla. This statement is supported not only by the comprehensive Quality Information Document (Zacharioudaki et al., 2022a) but also by the 12-year skill assessment conducted against in situ hourly observations from Melilla coastal buoy (Annex 5a~~3~~). The comparison yielded a correlation coefficient of 0.96~~5~~ and revealed a slight underestimation of extreme SWH$_{o}$ values. To overcome such a drawback, future works should include the implementation of a dynamical downscaling methodology to improve ~~the~~ wave reanalysis accuracy at finer coastal scales (Vannucchi et al., 2021). Of course, this would necessarily require finding the right trade-off between adequate spatial resolutions and the available in-house computational resources. Complementarily, additional efforts should be devoted to assessing the dominant modes of extreme waves variability and their relationship with the most important climatic indices since this could enhance the prognostic skills of extreme wave events and benefit the adaptation plans in the entire Spanish harbour system.

Finally, it is worth mentioning that most of the outcomes derived from this~~e present~~ work could not only feed the incoming climate change observatory for the Spanish ports (which should be fully operational by 2025) but also be integrated into tailored multi-hazard early warning systems. They would act as a key component of robust capacity analysis frameworks, covering a wide range of dimensions, such as legislative, planning, infrastructure, technical, scientific and institutional partnerships (Haigh et al., 2018). Special attention should be focused on the thorough revision of security protocols and the implementation of mitigation plans within the harbour territory based on the updated return periods presented in this work. The design lifetime risk should be recalculated accordingly as coastal structures in the vicinity of the harbour must resist growing stresses during their lifespan and operations, such as wave overtopping, floodings or resonance, to name a few. ~~Within this context,~~ While the current port layout configuration must be adapted to the increasing frequency and magnitude of these stressors, future maritime facilities at Melilla harbour should be wisely designed and constructed taking into account these outcomes in order to withstand extreme wave regimes imposed by the changing marine environment (Vanem et al., 2019). Albeit methodologically robust, the return periods exposed in this work are based on short (12-year) time series of

Con formato: Subíndice

Con formato: Subíndice

Con formato: Fuente: (Predeterminada) Times New Roman, 10 pto, Color de fuente: Automático, Diseño: Claro

Con formato: Fuente: (Predeterminada) Times New Roman, 10 pto, Color de fuente: Automático, Diseño: Claro

Con formato: Fuente: (Predeterminada) Times New Roman, 10 pto, Color de fuente: Automático, Diseño: Claro

Con formato: Fuente: (Predeterminada) Times New Roman, 10 pto, Color de fuente: Automático, Diseño: Claro

Con formato: Fuente: Times New Roman, 10 pto, Color de fuente: Automático, Diseño: Claro

Con formato: Fuente: Times New Roman, 10 pto, Color de fuente: Automático, Diseño: Claro

Con formato: Fuente: Times New Roman, 10 pto, Color de fuente: Automático, Diseño: Claro

Con formato: Fuente: Times New Roman, 10 pto, Color de fuente: Automático, Diseño: Claro

Con formato: Fuente: Sin Cursiva, Color de fuente: Automático

Con formato: Fuente: Sin Cursiva, Color de fuente: Automático

Con formato: Fuente: Sin Cursiva, Color de fuente: Automático

Con formato: Fuente: Sin Cursiva, Color de fuente: Automático quality-controlled in situ wave observations. Therefore, they should be further complemented with return periods computed by means of longer modelled time series from very high-resolution wave reanalysis.

Con formato: Fuente: Sin Cursiva, Color de fuente: Automático

Data availability

The model and observation products used in this study from both the Copernicus Marine Service and other sources are listed in Table 1.

Author contributions

PL, MA, PG, FM, AMM, BPG and, SPR and MIR conducted the pilot study through fruitful discussions in the framework of working team meetings. PL: designed the experiment, analysed the long-term wave trends, created the figures, and prepared successivea first versions of the draft with inputs from severalall co-authors. MA: conducted a bibliographic revision of extreme metocean events previously occurred in the Mediterranean Sea. PG: computed the return period before and after the record-breaking event. FM: extracted time series from Puertos del Estado internal database and prepared diverse in situ sensors datasets. AMM: downloaded and post-processed the reanalysis dataset. BPG: proposed the agitation and infragravity band study in the port, and analysed the corresponding tide-gauge records. SPR: provided a tailored coastline for Melilla harbour and analysed the atmospheric driving mechanisms during the event. MIR: applied a quality control for historical time series of wave parameters from Melilla coastal buoy. Finally, severalall authors participated in successive iterations, the drafting and revision of the manuscript.

Competing interests

The contact author has declared that none of the authors has any competing interests. Disclaimer. Publisher's note: Copernicus Publications remains neutral with regard to jurisdictional claims in published maps and institutional affiliations.

Acknowledgments

The authors are grateful to the Copernicus Marine Service for the data provision.

References

Álvarez-Fanjul, E., Pérez Gómez, B., de Alfonso Alonso-Muñoyerro, M., Lorente, P., García Sotillo, M., Lin-Ye, J., Aznar Lecocq, R., Ruíz Gil de la Serna, M., Pérez Rubio, S., Clementi, E., Coppini, G., García-León, M., Fernandes, M., García

Valdecasas, J., García Valdecasas, J.M., Santos Muñoz, D., Luna Rico, M.Y., Mestres, M., Molina, R., Tintoré, J., Mourre, B., Masina, S., Mosso, C., Reyes, E., Santana, A.: Western Mediterranean record-breaking storm Gloria: An integrated assessment based on models and observations, J. Oper. Oceanogr, doi:10.1080/ 1755876X.2022.2095169, 2022.

Amarouche, K., Akpınar, A. and Semedo, A.: Wave storm events in the Western Mediterranean Sea over four decades, Ocean Modelling, 170, 101933, ISSN 1463-5003, doi:10.1016/j.ocemod.2021.101933, 2022a.

Amarouche, K., Bingölbali, B. and Akpinar, A.: New wind-wave climate records in the Western Mediterranean Sea, Clim Dyn, 58, 1899–1922, doi:10.1007/s00382-021-05997-1, 2022b.

Amores, A., Marcos, M., Carrió, D. S., and Gómez-Pujol, L.: Coastal impacts of storm gloria over the northwestern mediterranean, Nat. Hazards Earth Syst. Sci., 20, 1955–1968, doi: 10.5194/nhess-20-1955-2020, 2020.

Aucan, J. and Ardhuin, F.: Infragravity waves in the deep ocean: an upward revision, Geophysical Research Letters, 40 (13), 3435-3439, doi: 10.1002/grl.50321, 2013.

Barbariol, F., Davison, S., Falcieri, F.M., Ferretti, R., Ricchi, A., Sclavo, M. and Benetazzo, A.: Wind Waves in the Mediterranean Sea: An ERA5 Reanalysis Wind-Based Climatology, Front. Mar. Sci., 8, 760614, doi: 10.3389/fmars.2021.760614, 2021.

Barriopedro, D., García-Herrera, R., Lupo, A.R. and Hernández, E.: A climatology of Northern Hemisphere blocking, J. Climate, 19, 1042–1063, doi:10.1175/JCLI3678.1, 2006.

Bellafont, F.: Role of infragravity waves on port agitation during storm events, Civil Engineering, Université de Pau et des Pays de l'Adour. English. NNT: 2019PAUU3047. Tel-02881282, 2019.

Bellotti, G. and Franco, L.: Measurement of long waves at the harbor of Marina di Carrara, Italy, Ocean Dynamics. 61, 2051–2059, doi:10.1007/s10236-011-0468-6, 2011.

~~Berta, M., Corgnati, L., Magaldi, M., Griffa, A., Mantovani, C. Rubio, A. Reyes, E. and Mader, J.: Small scale ocean weather during an extreme wind event in the Ligurian Sea. Journal of Operational Oceanography (Copernicus Marine Service Ocean State Report, Issue 4), Volume: 13:sup1, 149-154, doi:10.1080/1755876X.2020.1785097, 2020.~~

Bensoussan, N., Chiggiato, J., Nardelli, B.B., Pisano, A. and Garrabou, J.: Insights on 2017 Marine Heat Waves in the Mediterranean Sea, Journal of Operational Oceanography (Copernicus Marine Service Ocean State Report, Issue 3), ~~Volume:~~ 12 (~~:sup~~1), 101-108, doi: 10.1080/1755876X.2019.1633075, 2019.

Berta, M., Corgnati, L., Magaldi, M., Griffa, A., Mantovani, C. Rubio, A. Reyes, E. and Mader, J.: Small scale ocean weather during an extreme wind event in the Ligurian Sea, Journal of Operational Oceanography (Copernicus Marine Service Ocean State Report, Issue 4), ~~Volume:~~ 13 (~~:sup~~1), 149-154, doi:10.1080/1755876X.2020.1785097, 2020.

Caloiero, T. and Aristodemo, F.: Trend Detection of Wave Parameters along the Italian Seas, Water, 13 (12), 1634, doi:10.3390/w13121634, 2021.

Con formato: Español (España)

Con formato: Español (España)

Con formato: Color de fuente: Automático

Con formato: Color de fuente: Automático

Con formato: Espacio Después: 0 pto, Interlineado: 1,5 líneas, Diseño: Claro

Con formato: Color de fuente: Automático

Con formato: Color de fuente: Automático

Con formato: Color de fuente: Automático

Camus, P., Tomás, A., Izaguirre, C., Rodríguez, B., Díaz-Hernández, G. and Losada, I.: Probabilistic assessment of port operability under climate change, Coastal management, environment, and risk, doi:10.9753/icce.v36.risk.54, ~~Nº 36, ~~2018.

Casas-Prat, M. and Sierra, J.P.: Trend analysis of wave direction and associated impacts on the Catalan coast,~~.~~ Climatic Change, 115, 667–691, doi:10.1007/s10584-012-0466-9, 2012.

Cavaleri, L., Bertotti, L., Torrisi, L., Bitner-Gregersen, E., Serio, M., and Onorato, M.: Rogue waves in crossing seas: The Louis Majesty accident, J. Geophys. Res., 117, C00J10, https://doi.org/10.1029/2012JC007923, 2012.

~~Chiggiato et al. 2023: ~~Chiggiato, J., Artale, V., de Madron, X.D., Schroeder, K., Taupier-Letage, I., Velaoras, D. and Vargas-Yáñez, M.: Recent changes in the Mediterranean Sea,~~.~~ In book: Oceanography of the Mediterranean Sea, An introductory guide. Elsevier 2023, 289-334. doi: 10.1016/B978-0-12-823692-5.00008-X, 2023.

Clementi, E., Korres, G., Cossarini, G., Ravdas, M., Federico, I., Goglio, A.C., Salon, S., Zacharioudaki, A., Pattanaro, M. and Coppini, G.: The September 2020 Medicane Ianos predicted by the Mediterranean Forecasting systems,~~.~~ Ocean State Report Issue 6, Journal of operational oceanography, doi:10.1080/1755876X.2022.2095169, 2022.

Copernicus Marine In situ Team. 2017. Copernicus in Situ TAC, Real Time Quality Control for WAVES. Toulouse, France: Copernicus in situ TAC, 1–19. doi:10.13155/46607.

Costas, R., Figuero, A., Sande, J., Peña, E., and Guerra, A.: The influence of infragravity waves, wind, and basin resonance on vessel movements and related downtime at the Outer Port of Punta Langosteira, Spain,~~.~~ Applied Ocean Research, 129, 103370, doi:10.1016/j.apor.2022.103370, 2022.

Dayan, H., McAdam, R., Juza, M., Masina, S. and Speich, S.: Marine heat waves in the Mediterranean Sea: An assessment from the surface to the subsurface to meet national needs,~~.~~ Front. Mar. Sci., 10:1045138, doi: 10.3389/fmars.2023.1045138, 2023.

De Alfonso, M., García-Valdecasas, J.M., Aznar, R., Pérez-Gómez, B., Rodríguez, P., de los Santos, F.J. and Álvarez-Fanjul, E.: Record wave storm in the Gulf of Cadiz over the past 20 years and its impact on harbours,~~.~~ Copernicus Marine Service Ocean State Report, Issue 4, Journal of Operational Oceanography, 13 (~~:sup~~1), Section 4.6, ~~S~~137-~~S~~144, doi~~DOI~~: 10.1080/1755876X.2020.1785097, 2020.

De Alfonso, M., Lin-Ye, J., García-Valdecasas, J.M., Pérez-Rubio, S., Luna, M.Y., Santos-Muñoz, D., Ruiz, M.I., Pérez-Gómez, B. and Álvarez-Fanjul. E.: Storm Gloria: sea state evolution based on in situ measurements and modelled data and its impact on extreme values,~~.~~ Front. Mar. Sci., 8, ~~:~~1–17, doi:10. 3389/fmars.2021.646873, 2021.

De Leo, F., Briganti, R. and Besio, G.: Trends in ocean waves climate within the Mediterranean Sea: a review, Climate Dynamics, doi:10.1007/s00382-023-06984-4, 2023.

Denaxa, D., Korres, G., Sotiropoulou, M. and Lecci, R.: EU Copernicus Marine Service Product User Manual for the Mediterranean Sea Waves Reanalysis MEDSEA_MULTIYEAR_WAV_006_012, Issue: 2.2, Mercator Ocean International, https://catalogue.marine.copernicus.eu/documents/PUM/CMEMS-MED-PUM-006-012.pdf (last access: 11~~2~~ January~~une~~ 2024~~3~~), 2022.

ECCLIPSE website: https://ecclipse.eu/, last access: 11 January 2024~~18 July 2023~~.

Con formato: Fuente: (Predeterminada) Times New Roman, 10 pto
Con formato: Fuente: (Predeterminada) Times New Roman, 10 pto
Con formato: Inglés (Reino Unido)
Con formato: Fuente: (Predeterminada) Times New Roman, 10 pto
Con formato: Inglés (Reino Unido)
Con formato: Fuente: (Predeterminada) Times New Roman, 10 pto
Con formato: Fuente: (Predeterminada) Times New Roman, 10 pto
Con formato: Fuente: (Predeterminada) Times New Roman, Color de fuente: Automático
Con formato: Fuente: Times New Roman, Color de fuente: Automático, Diseño: Claro
Con formato: Fuente: Times New Roman, Color de fuente: Automático, Diseño: Claro
Con formato: Fuente: Times New Roman, Color de fuente: Automático, Diseño: Claro
Con formato: Fuente: Times New Roman, Color de fuente: Automático, Diseño: Claro
Con formato: Fuente: Times New Roman, Sin Cursiva, Color de fuente: Automático, Diseño: Claro
Con formato: Fuente: Times New Roman, Color de fuente: Automático, Diseño: Claro
Con formato: Fuente: Times New Roman, Color de fuente: Automático, Diseño: Claro

Emery, W.J. and Thompson, R.E.: Data Analysis Methods in Physical Oceanography, Elsevier Science, ISBN 9780080477008, 654 pages, Amsterdam, 2001.

EU Copernicus Marine Service Product: Atlantic Iberian Biscay Irish Ocean- In-Situ Near Real Time Observations, Mercator Ocean International [data set], https://doi.org/10.48670/moi-00043, 2022a.

EU Copernicus Marine Service Product: Mediterranean Sea Waves Reanalysis, Mercator Ocean International [data set], https://doi.org/10.25423/cmcc/medsea_multiyear_wav_006_012, 2022b.

Elgar, S., Herbers, T.H.C., Okihiro, M., Oltman-Shay, J. and Guza, R.T.: Observations of infragravity waves,~~.~~ J. Geophys. Res., 97 (C10), 15573–15577, 1992.

Erikson, L., Morim, J., Hemer, M. et al.: Global Ocean wave fields show consistent regional trends between 1980 and 2014 in a multi-product ensemble,~~.~~ Commun Earth Environ 3, 320, doi:10.1038/s43247-022-00654-9, 2022.

Eyring, V., N.P. Gillett, K.M. Achuta Rao, R. Barimalala, M. Barreiro Parrillo, N. Bellouin, C. Cassou, P.J. Durack, Y. Kosaka, S. McGregor, S. Min, O. Morgenstern, and Y. Sun~~, 2021~~: Human Influence on the Climate System,~~.~~ In Climate Change 2021: The Physical Science Basis. Contribution of Working Group I to the Sixth Assessment Report of the Intergovernmental Panel on Climate Change [Masson-Delmotte, V., P. Zhai, A. Pirani, S.L. Connors, C. Péan, S. Berger, N. Caud, Y. Chen, L. Goldfarb, M.I. Gomis, M. Huang, K. Leitzell, E. Lonnoy, J.B.R. Matthews, T.K. Maycock, T. Waterfield, O. Yelekçi, R. Yu, and B. Zhou (eds.)]. Cambridge University Press, Cambridge, United Kingdom and New York, NY, USA, 423–552, doi: 10.1017/9781009157896.005, 2021.

Fanti, V., Ferreira, Ó., Kümmerer, V. and Loureiro, C~~ et al~~.: Improved estimates of extreme wave conditions in coastal areas from calibrated global reanalyses,~~.~~ Commun Earth Environ, 4, 151, doi:10.1038/s43247-023-00819-0, 2023.

García-Valdecasas, J., Pérez Gómez, B., Molina, R., Rodríguez, A., Rodríguez, D., Pérez, S., Campos, A., Rodríguez-Rubio, P., Gracia, S., Ripollés, L., Terrés Nicoli, J.M., de los Santos, F.J. and Álvarez-Fanjul, E.~~,~~:~~et al.:~~ Operational tool for characterizing high-frequency sea level oscillations, Nat. Hazards, 106, 1149–1167, doi:10.1007/s11069-020-04316-x, 2021.

Garrabou, J., Gómez-Gras, D., Medrano, A. et al.: Marine heatwaves drive recurrent mass mortalities in the Mediterranean Sea,~~.~~ Global Change Biology, 28, 5708– 5725, doi:10.1111/gcb.16301, 2022.

Giesen, R., Clementi, E., Bajo, M., Federico, I., Stoffelen, A. and Santoleri, R.: The November 2019 record high water levels in Venice, Italy,~~.~~ Journal of Operational Oceanography (Copernicus Marine Service Ocean State Report, Issue 5), ~~Volume:~~ 14 (~~:sup~~1), 156-162, doi: 10.1080/1755876X.2021.1946240, 2021.

Goda, Y.: On the methodology of selecting design wave height. Coastal Engineering Proceedings, 1 (21), 1988.

~~Gómez Lahoz, G. and Carretero Albiach, J.C.: Wave forecasting at the Spanish coasts, Journal of Atmospheric and Ocean Science, 10:4, 389-405, doi: 10.1080/17417530601127522, 2005.~~

~~Guizien, K.: Spatial variability of wave conditions in the Gulf of Lions (NW Mediterranean Sea). Vie et milieu - life and environment, 59 (3/4): 261-270, 2009.~~

Con formato: Fuente: (Predeterminada) Times New Roman, 10 pto, Color de fuente: Automático, Ligaduras: Ninguna

Con formato: Fuente: (Predeterminada) Times New Roman, Color de fuente: Automático

Con formato: Fuente: (Predeterminada) Times New Roman, 10 pto, Color de fuente: Automático, Ligaduras: Ninguna

Con formato: Fuente: (Predeterminada) Times New Roman, Color de fuente: Automático

Con formato: Fuente: (Predeterminada) Times New Roman, 10 pto, Color de fuente: Automático, Ligaduras: Ninguna

Con formato: Fuente: (Predeterminada) Times New Roman, Color de fuente: Automático

Con formato: Fuente: (Predeterminada) Times New Roman, 10 pto, Color de fuente: Automático, Ligaduras: Ninguna

Con formato: Fuente: (Predeterminada) Times New Roman, 10 pto, Color de fuente: Automático, Ligaduras: Ninguna

Con formato: Fuente: (Predeterminada) Times New Roman, 10 pto

Con formato: Español (España)

Con formato: Español (España)

Gutiérrez-Serret, R., Grassa, J.M., Grau, J.I.: Breakwater development in Spain. The last ten years,~~.~~ Proceeding presented at Coasts, Marine Structures and Breakwaters: Adapting to Change, 9th International Conference organised by the Institution of Civil Engineers, Edinburgh, Scotland, UK, 16-18 September 2009.

Guza, R. T., and Thornton, E. B.: Swash oscillations on a natural beach, Journal of Geophysical Research: Oceans, 87(C1), 483-491, 1982.

Haigh, R., Amaratunga, D. and Hemachandra, K.: A capacity analysis framework for multi-hazard early warning in coastal communities,~~.~~ Procedia Engineering, 212, 1139-1146, doi:10.1016/j.proeng.2018.01.147, 2018.

Harley, M.: Coastal storm definition, In Coastal storms: processes and impacts, 1–21, Ed. John Wiley & Sons, 2017.

Hochman, A., Marra, F., Messori, G., Pinto, J.G., Raveh-Rubin, S., Yosef, Y. and Zittis, G.: Extreme weather and societal impacts in the eastern Mediterranean,~~.~~ Earth System Dynamics, 13, 749-777, doi:10.5194/esd-13-749-2022, 2022.

Hurrell, J.W. and Deser, C.: North Atlantic climate variability: The role of the North Atlantic Oscillation, J. Mar. Syst., 78, 28–41, doi: 10.1016/j.jmarsys.2009.11.002, 2009.

Inch, K., Davidson, M., Masselink, G. and Russell, P.: Observations of nearshore infragravity wave dynamics under high energy swell and wind-wave conditions, Continental Shelf Research, 138, 19-31, doi:10.1016/j.csr.2017.02.010, 2017.

In Situ TAC partners: EU Copernicus Marine Service Product User Manual for the Atlantic Iberian Biscay Irish Ocean- In-Situ Near Real Time Observations, INSITU_IBI_PHYBGCWAV_DISCRETE_MYNRT_013_033, Issue: 1.14, Mercator Ocean International, https://catalogue.marine.copernicus.eu/documents/PUM/CMEMS-INS-PUM-013-030-036.pdf (last access: 11 January 2024~~2 June 2023~~), http://dx.doi.org/10.13155/43494, 2022.

Intergovernmental Panel on Climate Change (IPCC). The Ocean and Cryosphere in a Changing Climate: Special Report of the Intergovernmental Panel on Climate Change. Cambridge: Cambridge University Press. doi:10.1017/9781009157964, 2022.

Izaguirre, C., Losada, I.J., Camus, P. et al.: Climate change risk to global port operations,~~.~~ Nat. Clim. Chang., 11, 14–20, doi:10.1038/s41558-020-00937-z, 2021.

Juza, M. and Tintoré, J.: Multivariate Sub-Regional Ocean Indicators in the Mediterranean Sea: From Event Detection to Climate Change Estimations, Front. Mar. Sci., 8, 610589, https://doi.org/10.3389/fmars.2021.610589, 2021.

Kautz, L.A., Martius, O., Pfahl, S., Pinto, J.G., Ramos, A.M., Sousa, P.M. and Woollings, T.: Atmospheric blocking and weather extremes over the Euro-Atlantic sector – a review, Weather Clim. Dynam., 3, 305–336, doi:10.5194/wcd-3-305-2022, 2022.

Kendall, M.G. Rank Correlation Methods; Hafner Publishing Company: New York, NY, USA, 1962.

Con formato: Color de fuente: Automático

Con formato: Color de fuente: Automático

Con formato: Color de fuente: Automático

Con formato: Color de fuente: Automático

Con formato: Color de fuente: Automático

Con formato: Color de fuente: Automático

Con formato: Color de fuente: Automático

Con formato: Sangría: Izquierda: 0 cm, Primera línea: 0 cm, Espacio Después: 0 pto, Interlineado: 1,5 líneas

Con formato: Sangría: Izquierda: 0 cm, Primera línea: 0 cm, Espacio Después: 0 pto, Interlineado: 1,5 líneas

Kokkini, Z. and Notarstefano, G.: Unusual salinity pattern in the South Adriatic Sea in 2016. Copernicus Marine Service Ocean State Report, Journal of Operational Oceanography, 11 (~~:sup~~1), ~~S~~130-~~S~~131, doi: 10.1080/1755876X.2018.1489208, 2018.

Konisky, D. M., Hughes, L., and Kaylor, C.H.: Extreme weather events and climate change concern,~~.~~ Clim. Change, 134, 533–547, doi: 10.1007/s10584-015-1555-3, 2015.

Lashley C.H., Bricker J.D., Van der Meer, J., Altomare, C. and Suzuki, T.: Relative Magnitude of Infragravity Waves at Coastal Dikes with Shallow Foreshores: A Prediction Tool, Journal of Waterway, Port, Coastal, and Ocean Engineering, 146 (5), doi:10.1061/(ASCE)WW.1943-5460.00005, 2020.

Linnenluecke, M. K., Griffiths, A., and Winn, M.: Extreme weather events and the critical importance of anticipatory adaptation and organizational resilience in responding to impacts,~~.~~ Bus. Strat. Environ., 21, 17–32, doi: 10.1002/bse.708, 2012.

López, M. and Iglesias, G.: Long wave effects on a vessel at berth, Applied Ocean Research, 47, 63-72, doi:10.1016/j.apor.2014.03.008, 2014.

Lorente, P., Lin-Ye, J., García-León, M., Reyes, E., Fernandes, M., Sotillo, M.G., Espino, M., Ruiz, M. I., Gracia, V., Pérez, S., Aznar, R., Alonso-Martirena, A., and Álvarez-Fanjul, E.: On the Performance of High Frequency Radar in the Western Mediterranean During the Record-Breaking Storm Gloria, Front. Mar. Sci., 8, 645762, doi:10.3389/fmars.2021.645762, 2021.

Lupo, A.R.: Atmospheric blocking events: a review, Ann N Y Acad Sci. 2021 Nov, 1504(1). 5-24, doi: 10.1111/nyas.14557, 2020.

Mackay, E. and Johanning, L.: Long-term distributions of individual wave and crest heights, Ocean Eng., 165, 164-183, 10.1016/j.oceaneng.2018.07.047, 2018a.

Mackay, E. and Johanning, L.: A generalised equivalent storm model for long-term statistics of ocean waves, Coastal Engineering, 140, 411-428, doi: 10.1016/j.coastaleng.2018.06.001, 2018b.

Mann, H.B. Nonparametric tests against trend,~~.~~ Econometrica, 13, 245–259, 1945.

McComb, J.: Modelling long wave generation and propagation around and within ports,~~.~~ Proc. 2011 Coasts and Ports Conf. Perth, Australia, 2011.

McComb, P., Zyngfogel, R., and Pérez-Gomez, B.: Predicting infragravity waves in harbours - an evaluation of published equations and their use in forecasting operational thresholds, Coastal Engineering Proceedings, 36v, waves.7, doi:10.9753/icce.v36v.waves.7, 2020.

~~Mann, H.B. Nonparametric tests against trend. Econometrica, 13, 245–259, 1945.~~

Milglietta, M. M. and Rotunno, R.: Development mechanisms for Mediterranean tropical-like cyclones (medicanes), Q. J. Roy. Meteorol. Soc., 145, 1444–1460, 2019.

Con formato: Color de fuente: Automático

Con formato: Color de fuente: Automático

Con formato: Fuente: (Predeterminada) Times New Roman, Color de fuente: Automático

Con formato: Fuente: (Predeterminada) Times New Roman, 10 pto, Color de fuente: Automático, Ligaduras: Ninguna

Con formato: Fuente: (Predeterminada) Times New Roman, Color de fuente: Automático

Con formato: Fuente: (Predeterminada) Times New Roman, 10 pto, Color de fuente: Automático, Ligaduras: Ninguna

Con formato: Fuente: (Predeterminada) Times New Roman, Color de fuente: Automático

Con formato: Fuente: (Predeterminada) Times New Roman, 10 pto, Color de fuente: Automático, Ligaduras: Ninguna

Con formato: Fuente: (Predeterminada) Times New Roman, Color de fuente: Automático

Con formato: Fuente: (Predeterminada) Times New Roman, 10 pto, Color de fuente: Automático, Ligaduras: Ninguna

Con formato: Fuente: (Predeterminada) Times New Roman, Color de fuente: Automático

Con formato: Fuente: (Predeterminada) Times New Roman, 10 pto, Color de fuente: Automático, Ligaduras: Ninguna

Con formato: Fuente: (Predeterminada) Times New Roman, Color de fuente: Automático

Con formato: Fuente: (Predeterminada) Times New Roman, 10 pto, Color de fuente: Automático, Ligaduras: Ninguna

Con formato: Fuente: (Predeterminada) Times New Roman, Color de fuente: Automático

Con formato: Fuente: (Predeterminada) Times New Roman, 10 pto, Color de fuente: Automático, Ligaduras: Ninguna

Con formato: Fuente: (Predeterminada) Times New Roman, Color de fuente: Automático

Con formato: Fuente: (Predeterminada) Times New Roman, Color de fuente: Automático

Con formato: Fuente: (Predeterminada) Times New Roman, Color de fuente: Automático

Con formato: Fuente: (Predeterminada) Times New Roman, Color de fuente: Automático

Con formato: Espacio Después: 0 pto, Interlineado: 1,5 líneas, Diseño: Claro

Morales-Márquez, V., Orfila, A., Simarro, G., and Marcos, M.: Extreme waves and climatic patterns of variability in the Eastern North Atlantic and Mediterranean Basins,. Ocean Sci., 16, 1385–1398, doi: 10.5194/os-16-1385-2020, 2020.

Naseef, T.M., Kumar, V.S., Joseph, J. et al.: Uncertainties of the 50-year wave height estimation using generalized extreme value and generalized Pareto distributions in the Indian Shelf seas, Nat. Hazards, 97, 1231–1251, doi:10.1007/s11069-019-03701-5, 2019.

Munk, W. H.: On the wind-driven ocean circulation, J. Atmos. Sci., 7, 80–93, https://doi.org/10.1175/1520-0469(1950)007<0080:OTWDOC>2.0.CO;2, 1950.

Notarstefano, G., Menna, M. and Legeais, J.F.: Reversal of the Northern Ionian circulation in 2017,. Ocean State Report, 3, Journal of Operational Oceanography, 12 (:sup1), S108-S111, doi: 10.1080/1755876X.2019.1633075, 2019.

Okihiro, M., Guza, R.T. and Seymour, R.J.: Excitation of seiche observed in a small harbor,. J. Geophys. Res., 98, 18.201–18.211, 1993.

Pérez-Gómez, B., Vela, J., and Alvarez-Fanjul, E.: A new concept of multi-‒purpose sea level station: example of implementation in the REDMAR network,. In: Proceedings of the Fifth International Conference on EuroGOOS, May 2008: Coastal to global operational oceanography: achievements and challenges, Exeter, 2008.

Pérez-Gómez, B., A. Payo, D. López, P.L. Woodworth and E. Alvarez-Fanjul: Overlapping sea level time series measured using different technologies: an example from the REDMAR Spanish network, Nat. Hazards Earth Syst. Sci., 14, 589-610, 2014.

Pérez-Gómez, B., García-León, M., García-Valdecasas, J., Clementi, E., Mösso Aranda, C., Pérez-Rubio, S., Masina, S., Coppini, G., Molina-Sánchez, R., Muñoz-Cubillo, A., García Fletcher, A., Sánchez González, J.F., Sánchez-Arcilla, A. and Álvarez-Fanjul, E.: Understanding Sea Level Processes During Western Mediterranean Storm Gloria,. Front. Mar. Sci. 8:647437. doi: 10.3389/fmars.2021.647437, 2021.

Portillo Juan, N., Negro Valdecantos, V., del Campo, J.M.: Review of the Impacts of Climate Change on Ports and Harbours and Their Adaptation in Spain,. Sustainability, 14, 7507, doi:10.3390/su14127507, 2022.

Radovic, V., and Iglesias, I.: Extreme weather events: definition, classification and guidelines towards vulnerability reduction and adaptation management,. Good Health Well Being, 68, 1–13, doi: 10.1007/978-3-319- 71063-1_68-1, 2018.

Ramirez-Llodra, E., De Mol, B., Company, J.B., Coll, M. and Sardà, F.: Effects of natural and anthropogenic processes in the distribution of marine litter in the deep Mediterranean Sea, Progress in Oceanography, 118, 273-287, doi:10.1016/j.pocean.2013.07.027, 2013.

Rex, D.F.: Blocking action in the middle troposphere and its effect upon regional climate, Tellus, 2, 275–301, doi: 10.1111/j.2153-3490.1950.tb00339.x, 1950.

Ribeiro, A.S., Lopes, C.L., Sousa, M.C., Gómez-Gesteira, M., Vaz, N., Dias, J.M.: Reporting Climate Change Impacts on Coastal Ports (NW Iberian Peninsula): A Review of Flooding Extent,. J. Mar. Sci. Eng., 11, 477, doi:10.3390/jmse11030477, 2023.

Romano-Moreno, E., Diaz-Hernandez, G., Lara, J.L. Tomás, A. and Jaime, F.F.: Wave downscaling strategies for practical wave agitation studies in harbours, Coastal Engineering, 175, 104140, ISSN 0378-3839, doi:10.1016/j.coastaleng.2022.104140, 2022.

Salvadori, G., Durante, F. and De Michele, C.: Multivariate return period calculation via survival functions,~~.~~ Water Resour. Res., 49, 2308–2311, doi:10.1002/wrcr.20204, 2013.

~~Samper, Y., Liste, M., Mestres, M., Espino, M., Sánchez-Arcilla, A., Sospedra, J., González-Marco, D., Ruiz, M.I., Álvarez Fanjul, E.: Water Exchanges in Mediterranean Microtidal Harbours, Water, 14 (13), doi:10.3390/w14132012, 2022.~~

~~Sánchez-Arcilla, A., Sierra, J.P., Brown, S., Casas-Prat, M., Nicholls, R.J., Lionello, P., and Conte, D.: A review of potential physical impacts on harbours in the Mediterranean Sea under climate change, Reg Environ Change, 16, 2471-2484, doi:10.1007/s10113-016-0972-9, 2016a.~~

Sánchez-Arcilla, A., García-León, M., Gracia, V., Devoy, R., Stanica, A., and Gault, J.: Managing coastal environments under climate change: Pathways to adaptation,~~.~~ Sci. Total Environ., 572, 1336–1352, doi: 10.1016/j.scitotenv.2016.01.124, 2016a~~b~~.

Sánchez-Arcilla, A., Sierra, J.P., Brown, S., Casas-Prat, M., Nicholls, R.J., Lionello, P., and Conte, D.: A review of potential physical impacts on harbours in the Mediterranean Sea under climate change, Reg. Environ. Change, 16, 2471–2484, doi:10.1007/s10113-016-0972-9, 2016b.

Scicchitano, G., Scardino, G., Monaco, C., Piscitelli, A., Milella, M., De Giosa, F. and Mastronuzzi, G.: Comparing impact effects of common storms and Medicanes along the coast of south-eastern Sicily, Marine Geology, 439, 106556, ISSN 0025-3227, doi:10.1016/j.margeo.2021.106556, 2021.

Sen, P.K. Estimates of the regression coefficient based on Kendall's tau. J. Am. Stat. Assoc., 63, 1379–1389, 1968.

Senechal, N., Coco, G., Bryan, K.R. and Holman, R.A.: Wave runup during extreme storm conditions, J. Geophys. Res., 116, C07032, doi:10.1029/2010JC006819, 2011.

Sierra, J. P., Casas-Prat, M., Virgili, M., Mösso, C., and Sánchez-Arcilla, A.: Impacts on wave-driven harbour agitation due to climate change in Catalan ports, Nat. Hazards Earth Syst. Sci., 15, 1695–1709, doi:10.5194/nhess-15-1695-2015, 2015.

Sierra, J.P., Genius, A. Lionello, P. Mestres, M. Mösso, C. and Marzo, L.: Modelling the impact of climate change on harbour operability: The Barcelona port case study, Ocean Engineering, 141, 64-78, doi:10.1016/j.oceaneng.2017.06.002, 2017.

Sotillo, M.G., Mourre, B., Mestres, M., Lorente, P., Liste, M., Aznar, R., et al.: How did existing operational ocean circulation models forecast a (record-breaking) Western Mediterranean Extreme Event?, Front. Mar. Sci. 81–23. doi: 10.1016/j.apor.2011.09.001, 2021.

Sousa, P.M., Barriopedro, D., García-Herrera, R., Woollings, T. and Trigo, R.M.: A New Combined Detection Algorithm for Blocking and Subtropical Ridges, J. Climate, 34, 7735–7758, doi:10.1175/JCLI-D-20-0658.1, 2021.

Con formato: Inglés (Reino Unido)

Con formato: Sangría: Izquierda: 0 cm, Primera línea: 0 cm, Espacio Después: 0 pto, Interlineado: 1,5 líneas

Soussi, A., Bersani, C., Sacile, R., Bouchta, D., El Amarti, A., Seghiouer, H., Nachite, D., and Al Miys, J.: Coastal Risk Modelling for Oil Spill in The Mediterranean Sea, Advances in Science, Technol. Eng. Syst. J., 5, 273–286, 2020.

Stockdon, H.F., Holman, R.A., Howd, P.A. and Sallenger Jr, A.H.: Empirical parameterization of setup, swash and runup. Coast. Eng., 53, 573–588, 2006.

Todd, D., Blanksby, A. and Schepis, J.: Verification of design life exposure and performance of a berm breakwater, Coastal Engineering, 2012.

Trigo, I.F., Davies, T.D. and Bigg, G.R. Objective climatology of cyclones in the Mediterranean region, J Clim, 12(6), 1685–1696, doi:10.1175/1520-0442(1999)0122.0.CO;2, 1999.

Tuel, A. and Eltahir, E.A.B.: Why Is the Mediterranean a Climate Change Hot Spot?,~~.~~ J. Climate, 33, 5829–5843, doi:10.1175/JCLI-D-19-0910.1, 2020.

Vanem, E., Fazeres-Ferradosa, T., Rosa-Santos, P. and Taveira-Pinto, F.: Statistical description and modelling of extreme ocean wave conditions,~~.~~ Proceedings of the Institution of Civil Engineers - Maritime Engineering, 172 (~~:~~4), 124-132, 2019.

Vannucchi, V., Taddei, S., Capecchi, V., Bendoni, M., Brandini, C.: Dynamical Downscaling of ERA5 Data on the North-Western Mediterranean Sea: From Atmosphere to High-Resolution Coastal Wave Climate,~~.~~ Journal of Marine Science and Engineering, 9 (2), ~~:~~208, doi:10.3390/jmse9020208, 2021.

Velpuri, M., Das, J. and Umamahesh, N.V. Spatio-temporal compounding of connected extreme events: Projection and hotspot identification, Environmental Research, 235, 116615, doi:10.1016/j.envres.2023.116615, 2023.

Verschuur, J., Koks, E.E. and~~&~~ Hall, J.W.: Ports' criticality in international trade and global supply-chains,~~.~~ Nat. Commun., 13, 4351, doi:10.1038/s41467-022-32070-0, 2022.

Verschuur, J., Koks, E.E., Li, S. et al.: Multi-hazard risk to global port infrastructure and resulting trade and logistics losses,~~.~~ Commun Earth Environ, 4, 5, doi:10.1038/s43247-022-00656-7, 2023.

WCPR website https://www.wcrp-climate.org/gc-extreme-events, last access: 11 January 2024~~18 July 2023~~.

Wehde, H., Schuckmann, K.V., Pouliquen, S., Grouazel, A., Bartolome, T., Tintore, J., De Alfonso Alonso-Muñoyerro, M., Carval, T., Racapé, V. and the INSTAC team: EU Copernicus Marine Service Quality Information Document for the Atlantic Iberian Biscay Irish Ocean- In-Situ Near Real Time Observations, INSITU_IBI_PHYBGCWAV_DISCRETE_MYNRT_013_033, Issue 2.2, Mercator Ocean International, https://catalogue.marine.copernicus.eu/documents/QUID/CMEMS-INS-QUID-013-030-036.pdf (last access:~~ 2 June 2023~~ 11 January 2024), 2022.

Wolff, C., Vafeidis, A. T., Muis, S., Lincke, D., Satta, A., Lionello, P., Jimenez, J. A., Conte, D., and Hinkel, J. A.: Mediterranean coastal database for assessing the impacts of sea-level rise and associated hazards, Sci. Data, 5, 180044, doi:10.1038/sdata.2018.44, 2018.

Zacharioudaki, A., Ravdas, M., Korres, G., and Goglio, A.C.: EU Copernicus Marine Service Quality Information Document for the Mediterranean Sea Waves Reanalysis. MEDSEA_MULTIYEAR_WAV_006_012, Issue: 2.2, Mercator Ocean

Con formato: Fuente: (Predeterminada) Times New Roman, Color de fuente: Automático

Con formato: Color de fuente: Automático

Con formato: Fuente: (Predeterminada) Times New Roman, Color de fuente: Automático

Con formato: Color de fuente: Automático

Con formato: Fuente: (Predeterminada) Times New Roman, Color de fuente: Automático

Con formato: Color de fuente: Automático

Con formato: Fuente: (Predeterminada) Times New Roman, Color de fuente: Automático

Con formato: Color de fuente: Automático

Con formato: Fuente: (Predeterminada) Times New Roman, Color de fuente: Automático

Con formato: Color de fuente: Automático

Con formato: Fuente: (Predeterminada) Times New Roman, Color de fuente: Automático

Con formato: Color de fuente: Automático

Con formato: Fuente: (Predeterminada) Times New Roman, Color de fuente: Automático

Con formato: Color de fuente: Automático

Con formato: Fuente: (Predeterminada) Times New Roman, Color de fuente: Automático

Con formato: Color de fuente: Automático

Con formato: Fuente: (Predeterminada) Times New Roman, Color de fuente: Automático

Con formato: Color de fuente: Automático

Con formato: Fuente: (Predeterminada) Times New Roman, Color de fuente: Automático

Con formato: Fuente: (Predeterminada) Times New Roman, Color de fuente: Automático

Con formato: Fuente: (Predeterminada) Times New Roman, Color de fuente: Automático

Con formato: Fuente: (Predeterminada) Times New Roman, Color de fuente: Automático

Con formato: Fuente: (Predeterminada) Times New Roman, Color de fuente: Automático

Con formato: Color de fuente: Automático

International, https://catalogue.marine.copernicus.eu/documents/QUID/CMEMS-MED-QUID-006-012.pdf (last access: 11 January 20242 June 2023), 2022a.

Zacharioudaki, A., Ravdas, M. and Korres, G.: Wave climate extremes in the Mediterranean Sea obtained from a wave reanalysis for the period 1993-2000,. Ocean state Report, Issue 6, Journal of Operational Oceanography, 2022b.

Tables

Product ref. no.	Product ID & type	Data access	Documentation
11	INSITU_IBI_PHYBGCWAV_DISCRETE_MYNRT_013_033, in situ observationsERA5 global reanalysis, numerical models	EU Copernicus Marine Service Product (2022a)Copernicus Climate Data Store: https://cds.climate.copernicus.eu/cdsapp#!/dataset/reanalysis-era5-single-levels?tab=form	PUM: In situ TAC partners (2022); QUID: Wehde et al. (2022)Product description: https://confluence.ecmwf.int/display/CKB/ERA5%3A+data+documentation

Tabla con formato

~~2~~	~~Puertos del Estado regional wave forecast model, numerical models~~	~~Puertos del Estado: https://portus.puertos.es https://portuscopia.puertos.es/~~	~~Product description: Gómez Lahoz and Carretero Albiach, 2005. https://www.puertos.es/es-es/Documents/Descripcion_Pred_Oleaje_en.pdf~~
2~~3~~	2_Hz data, high frequency sea level oscillations and agitation parameters from Melilla tide-gauge, in situ observations	Puertos del Estado websites: https://portus.puertos.es https://portuscopia.puertos.es/Catalog http://opendap.puertos.es/thredds/catalog/tidegauge_meli/catalog.html	Product description: García Valdecasas et al. (2021) https://bancodatos.puertos.es/BD/informes/INT_3.pdf
~~4~~	~~INSITU_IBI_PHYBGCWAV_DISCRETE_MYNRT_013_033, in situ observations~~	~~EU Copernicus Marine Service Product (2022a)~~	~~PUM: In situ TAC partners (2022); QUID: Wehde et al. (2022)~~
3	ERA5 global reanalysis, numerical models	Copernicus Climate Data Store: https://cds.climate.copernicus.eu/cdsapp#!/dataset/reanalysis-era5-single-levels?tab=form	Product description: https://confluence.ecmwf.int/display/CKB/ERA5%3A+data+documentation
4~~5~~	MEDSEA_MULTIYEAR_WAV_006_012, numerical models	EU Copernicus Marine Service Product (2022b)	PUM: Denaxa et al. (2022); QUID: Zacharioudaki et al. (2022a)

Table 1. Products from the Copernicus Marine Service and other complementary datasets used in this study, including the Product User Manual (PUM) and QUality Information Document (QUID). For complementary datasets, the link to the product description, data access and scientific references are provided. Last access for all web pages cited in this table: 11 January 2024~~12 June 2023~~.

Con formato: Inglés (Reino Unido)

Código de campo cambiado

Código de campo cambiado

Con formato: Español (España)

Con formato: Fuente: (Predeterminada) +Títulos (Times New Roman), Negrita

Work	Extreme event	Year	Location	Issue
Kokkini et al. (2018)	Anomaly of salinity	2016	Adriatic Sea	2
Bensoussan et al. (2019)	Marine heat wave	2017	Mediterranean Sea	3
Notarstefano et al. (2019)	Current reversal	2017	Ionian Sea	3
De Alfonso et al. (2020)	Emma Storm	2018	Gulf of Cadiz	4
Berta et al. (2020)	Extreme wind	2018	Ligurian Sea	4
Giesen et al. (2021)	Sea level rise	2019	Adriatic Sea	5
Álvarez-Fanjul et al. (2022)	Storm Gloria	2020	NW Mediterranean Sea	6
Clementi et al. (2022)	Medicane Ianos	2020	Ionian Sea	6

Table 2. Summary of recent studies (published in previous issues of the Ocean State Report) dealing with extreme metocean events in the Mediterranean Sea and adjacent areas.

Physical processes	Specific impacts	General impacts
Nonlinear interactions of wind short waves (5-30 s) Infragravity (IG) long waves (30-600 s) Resonance (seiche) Large water level fluctuations and strong horizontal currents	Excessive vessel motions at berth Restriction of (un)load operations Break of mooring lines / fenders Ship collision Damage to vessels / port facilities	Unsafe operations Inefficient port management Downtime of the facility Interruption of supply chain Economic losses

Table 3. Conceptual landscape of potential impacts on harbour operations and infrastructures during severe wave storms.

Con formato: Resaltar
Con formato: Resaltar
Con formato: Resaltar
Con formato: Resaltar
Con formato: Resaltar
Con formato: Resaltar
Con formato: Resaltar
Con formato: Resaltar
Con formato: Resaltar
Con formato: Resaltar
Con formato: Resaltar
Con formato: Resaltar
Con formato: Resaltar
Con formato: Resaltar

Source (Product ref)	Type	Location (coverage)	ParameterVariable (unit)	Temporal resolution Std	Time span usedP99	Spatial resolutionP 99.9
In situ sensor (1)	Buoy	Coastal location (2.94ºW – 35.33ºN)	SWH$_p$ (m)	Hourly0.59 0.87	2.92 6.29 2011-2022	Point-wise location4.44 7.27
			MWH$_o$ (m)			
			T$_m$mean period (s)			
			T$_p$ (s)			
			MWD$_p$ (º)			
In situ sensor (2)	Tide-gauge	Port location (2.93ºW – 35.29ºN)	Agitation (m)	Hourly	2011-2022	Point-wise location
			HFSLO$_{13}$ (m)			
			HFSLO$_{max}$ (m)			
			IGE (m^2·s)			
Numerical Model (3)	ERA5 reanalysis	Regional domain (19ºW - 5ºE 26ºN - 56ºN)	SLP (Pa)IG$_{max}$ (m)	Hourly0.05	1993-20220.28	0.25º0.44
			W10 (m·s^{-1})			0.25º
			SWH$_m$ (m)			0.5º
Numerical Model (4)	MED reanalysis	Subregional domain (6ºW - 1ºW 35ºN - 37ºN)	SWH$_m$ (m)	Hourly	1993-2022	1/24º
			MWD$_m$ (º)			
			agitation (m)	0.07	0.38	0.6

Table 42. Basic Complementary statistics information about the data sources used in this study. (mean, standard deviation, and diverse percentiles) for the significant wave height (SWH) and mean wave period hourly observations provided by Melilla coastal buoy (magenta square in Figure 1, b-c) for the period between 1 April 2008 and 31 December 2022. Infragravity waves maximum heigth (IG$_{max}$) and agitation data were provided by Melilla tide-gauge (magenta dot in Figure 1, b-c) for the entire period 2015-2022.

Con formato: Fuente: Negrita
Con formato: Centrado
Tabla con formato
Con formato: Fuente: Negrita
Con formato: Fuente: Negrita
Con formato: Subíndice
Con formato: Centrado
Con formato: Centrado
Con formato: Centrado
Con formato: Centrado
Con formato: Centrado
Con formato: Subíndice
Con formato: Centrado
Con formato: Subíndice
Con formato: Subíndice
Con formato: Centrado
Con formato: Centrado
Con formato: Centrado
Con formato: Centrado
Con formato: Centrado
Con formato: Centrado
Con formato: Centrado
Con formato: Centrado
Con formato: Centrado
Con formato: Centrado
Con formato: Centrado
Con formato: Centrado

Event	Date (hour)	SWH_o (m)	Time above P99 (h) *	MWH_o (m)	Mean period (s)	Peak period (s)	Mean direction (°)
E1	2016-02-21 (00)	5.25	16	9.46	7.15	9.13	63
E2	2017-02-21 (01)	5.21	57	7.22	6.83	9.25	66
E3	2017-03-15 (01)	5.05	27	7.79	6.99	9.98	51
E4	2017-04-21 (15)	5.36	58	6.97	7.03	9.34	69
E5	2019-03-27 (00)	5.21	31	8.03	6.88	9.91	69
E6	2021-03-20 (21)	5.09	14	6.83	6.91	9.69	55
E7	2022-04-04 (21)	7.32	37	12.11	9.42	10.75	55

Table 3. Characterization of the seven most extreme waves event registered by Melilla coastal buoy during the 12-year period analysed (2011-2022). *Consecutive hours above the 99th percentile of SWH_o.

Parameter ~~(unit)~~	~~20~~2011~~10~~-2021~~0~~	~~20~~2011~~10~~-2022	Decrease
~~Exceedance threshold (m)~~	~~2~~	~~2~~	
~~Minimum time between storms (days)~~	~~5~~	~~5~~	
~~Mean number of storms per year~~	~~9.73~~	~~10.12~~	
Weibull ~~distribution~~parameter: threshold~~alpha~~ (or	1.82	1.88~~90~~	------
Weibull ~~distribution~~parameter: scale~~beta~~	1.19~~3~~	1.10	------
Weibull ~~distribution~~parameter~~: gamma~~: shape (or	1.20~~14~~	1.07	------
Return period for events with SWH_o = 3 m ~~(years)~~	1.02~~3~~ years	1.02 years	0.00 %

Return period for events with SWH$_o$ SWH = 4 m (years)	1.3845 years	1.34 years	2.89 %
Return period for events with SWH$_o$ SWH = 5 m (years)	3.019 years	2.59 years	16.18 %
Return period for events with SWH = 6 m (years)	9.24	6.4	
Return period for events with SWH = 7 m (years)	30.41	17.75	
Return period for E1 extreme event (SWH$_o$ = 5.25 m)	4.00 years	3.19 years	20.25 %
Return period for E2 extreme event (SWH$_o$ = 5.21 m)	3.83 years	3.08 years	19.58 %
Return period for E3 extreme event (SWH$_o$ = 5.05 m)	3.25 years	2.69 years	17.23 %
Return period for E4 extreme event (SWH$_o$ = 5.36 m)	4.51 years	3.51 years	22.17 %
Return period for E5 extreme event (SWH$_o$ = 5.21 m)	3.83 years	3.08 years	19.58%
Return period for E6 extreme event (SWH$_o$ = 5.09 m)	3.38 years	2.78 years	17.75 %
Return period for E7 extreme events with (SWH$_o$ SWH =	15306.064	2451.9179 years	53.23 %

Table 45. Return period computed for two different periods, as derived from hourly in situ observations from Melilla coastal buoy. The long-term extreme sea state was characterised by using the Peak Over Threshold method with the fitting of a tThree-Parameter Weibull probability distribution to the observed significant wave height (SWH$_o$bservations).

IG wave height	Warning	Reactivity
< 0.10 m	Safe	Business as usual, well-tendered vessels
– 0.15 m	Caution	Additional management recommended
> 0.15 m	Extreme caution	Active management required
> 0.20 m	Danger	Evacuation of vessels from berths, port downtime

Table 6. Infragravity (IG) wave height thresholds used for port management.

Con formato: Centrado
Con formato: Centrado
Con formato: Centrado
Con formato: Centrado
Con formato: Sin Resaltar
Con formato: Sin Resaltar
Con formato: Sin Resaltar
Con formato: Sin Resaltar
Con formato: Sin Resaltar
Con formato: Sin Resaltar
Con formato: Sin Resaltar
Con formato: Sin Resaltar
Con formato: Sin Resaltar
Con formato: Sin Resaltar
Con formato: Sin Resaltar
Con formato: Sin Resaltar
Con formato: Sin Resaltar
Con formato: Sin Resaltar
Con formato: Sin Resaltar
Con formato: Sin Resaltar
Con formato: Sin Resaltar
Con formato: Sin Resaltar
Con formato: Sin Resaltar
Con formato: Sin Resaltar
Con formato: Sin Resaltar
Con formato: Sin Resaltar
Con formato: Sin Resaltar
Con formato: Centrado
Tabla con formato
Con formato: Resaltar
Con formato: Sangría: Izquierda: 0 cm

Figures

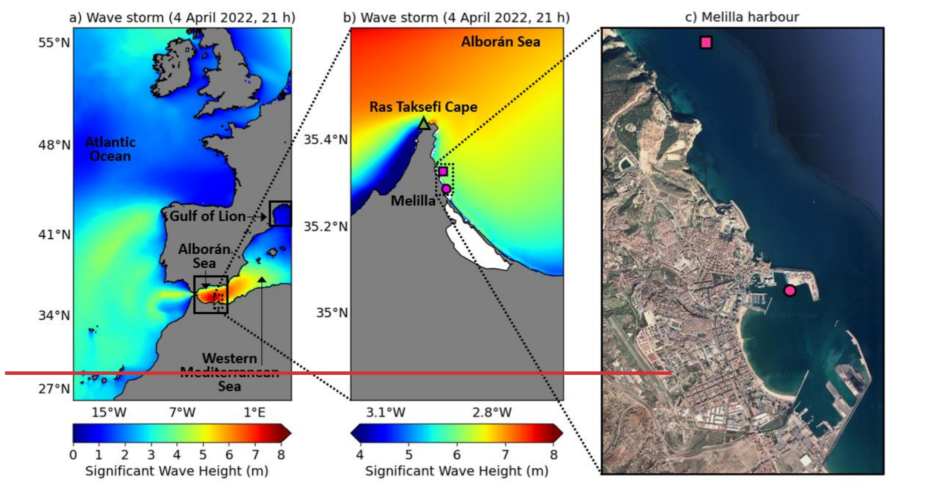

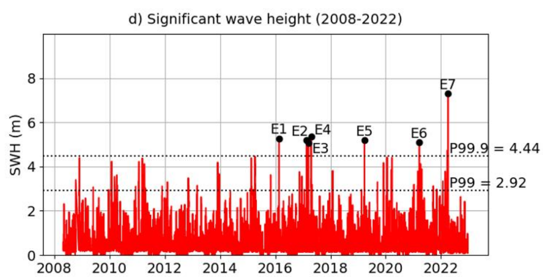

Event	Date (hour)	SWH (m)	Period (s)	Dir (°)
E1	2016-02-21 (00)	5.25	7.15	63
E2	2017-02-21 (02)	5.21	6.83	66
E3	2017-03-15 (01)	5.05	6.99	51
E4	2017-04-21 (15)	5.36	7.03	69
E5	2019-03-27 (00)	5.21	6.88	69
E6	2021-03-20 (21)	5.09	6.91	55
E7	2022-04-04 (21)	7.32	9.30	55

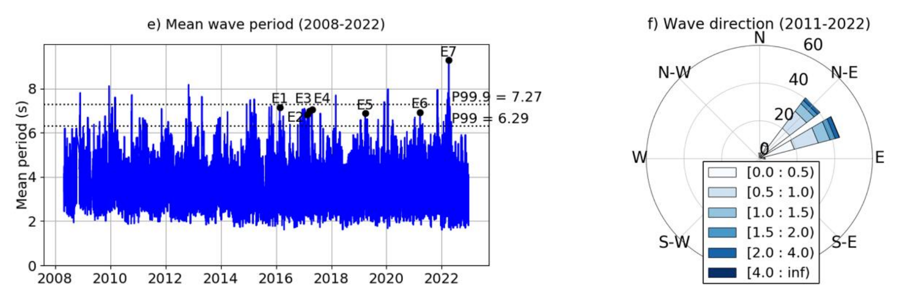

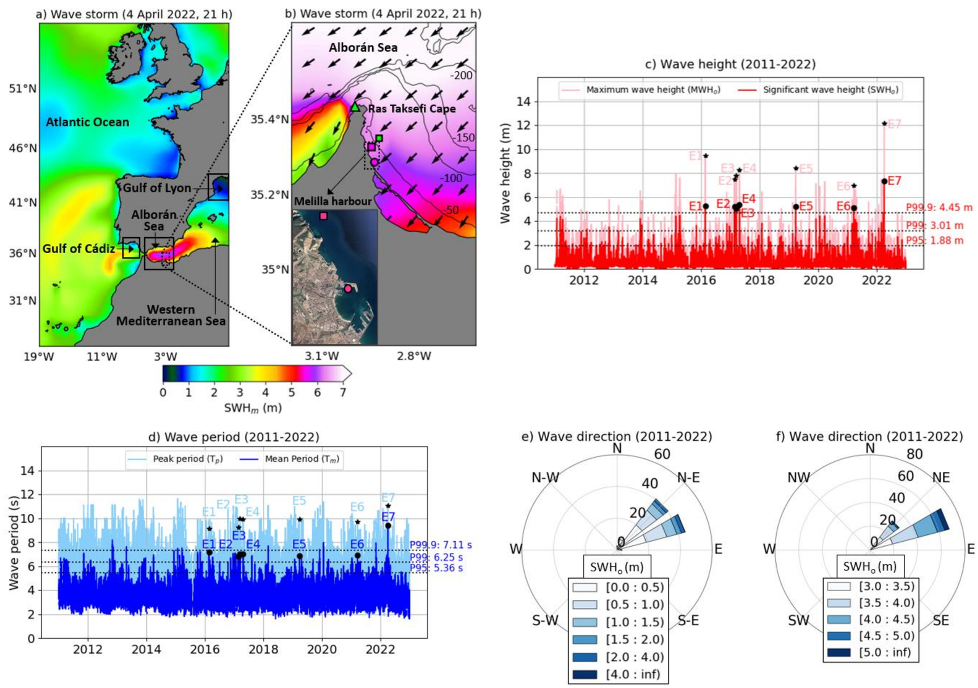

Figure 1. Wave storm in the SW Mediterranean Sea;. a) hHourly map (4 of April 2022, 21 h local time) of significant wave height (SWH$_m$) at synoptic (a) and coastal (b) scales scale during the peak storm as derived from ERA5 reanalysis -product ref. no. 3 (Table 1); b) hourly map of SWH$_m$ and MWD$_m$ at coastal scale during the peak storm as derived from MED reanalysis -product ref. no. 4 (Table 1). as predicted by the wave forecast model of Puertos del Estado -product ref. no. 2 (Table 1) . Isobath depths are labelled, every 50 m. Magenta dot and square represent Melilla tide-gauge and coastal buoy location, respectively. Green triangle and square indicates the location of Ras Taksefi Cape and the grid point of MED reanalysis closest to Melilla coastal buoy, respectively;; c) Google map illustrating the geometry and details of Melilla harbour. Magenta dot and square represent the tide-gauge and coastal buoy location, respectively; cd) Hhourly time series of SWH$_o$ and MWH$_o$ recorded at Melilla coastal buoy for 20201108-2022 -product ref. no. 14 (Table 1)-. Black dots and stars indicate the seven extreme events examined, labelled from E1 to E7.ose SWH events above The 99.9th (P99.9), and 99th (P99) and 95th (P95) percentiles are, represented by horizontal black dotted lines; . Table on the right gathers details about each event; de) Hourly time series of mean T$_m$ and T$_p$wave period for 20201108-2022 -product ref. no. 14 (Table 1)-; ef) Wave rose illustrating the

Con formato: Subíndice
Con formato: Subíndice
Con formato: Fuente: Negrita
Con formato: Fuente: Negrita
Con formato: Subíndice
Con formato: Subíndice
Con formato: Superíndice
Con formato: Superíndice
Con formato: Superíndice
Con formato: Subíndice
Con formato: Subíndice

main incoming directions (MWD$_0$) during the time period 2011-2022 -product ref. no. 14 (Table 1); f) Wave rose showing the MWD$_0$ associated with SWH$_0$ values above P99 (3.01 m) during 2011-2022..

Con formato: Subíndice

Con formato: Subíndice

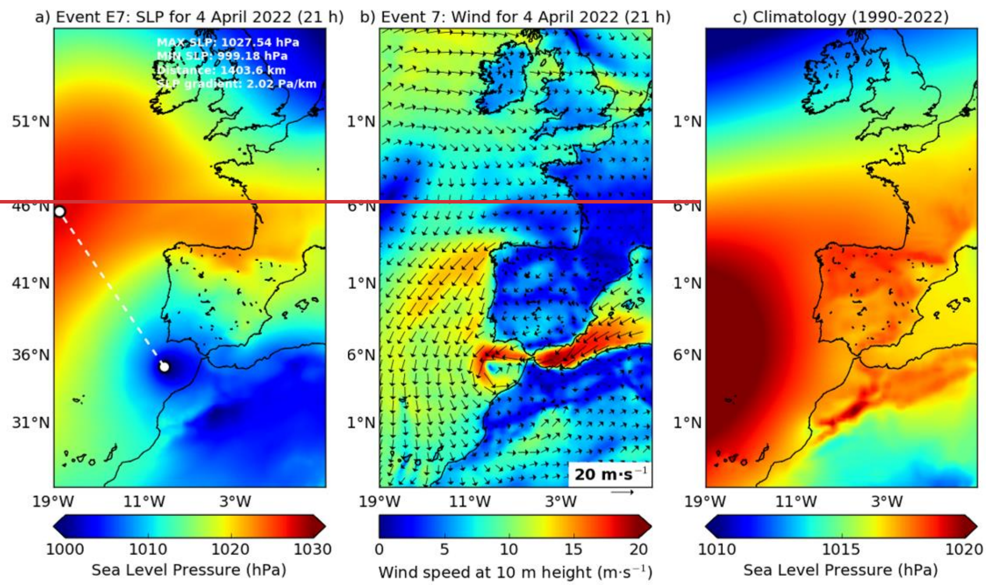
a) Event E7: SLP for 4 April 2022 (21 h)
MAX SLP: 1027.54 hPa
MIN SLP: 999.18 hPa
Distance: 1403.6 km
SLP gradient: 2.02 Pa/km
51°N
46°N
41°N
36°N
31°N
19°W
11°W
3°W
1000
1010
1020
1030
Sea Level Pressure (hPa)
b) Event 7: Wind for 4 April 2022 (21 h)
1°N
6°N
1°N
6°N
1°N
20 m·s^{-1}
19°W
11°W
3°W
0
5
10
15
20
Wind speed at 10 m height (m·s^{-1})
c) Climatology (1990-2022)
1°N
6°N
1°N
6°N
1°N
19°W
11°W
3°W
1010
1015
1020
Sea Level Pressure (hPa)

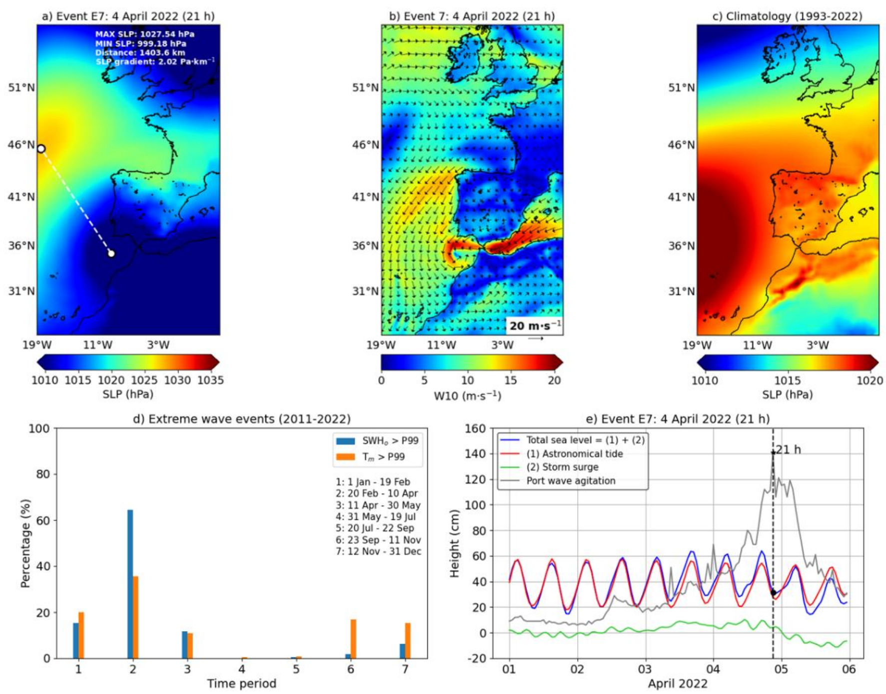

Figure 2. (a-b) Hourly synoptic patterns of sea level pressure (SLP) and wind at 10 m height (W10) during the extreme event E7; c) Climatology (199~~0~~3-2022) of SLP. Maps derived from ERA5 reanalysis -product ref. no. 3~~1~~ (Table 1); d) Bar diagram with the temporal distribution of events above the 99th percentile (P99) of significant wave height (SWH$_p$) and mean wave period T$_m$ derived from the 12-year time series (2011-2022) provided by Melilla coastal buoy (product ref. no. 1 in Table 1). The annual time span was divided into seven 50-day periods, except period 5 (20 July-22 September) which is composed by 65 days; e) Time series of total sea level height (blue line) and port agitation (black line) observations during E7 extreme event as provided by Melilla tide-gauge (product ref. no. 2 in Table 1). Astronomical tides and storm surge component (meteorological residuals) are represented by the red and green lines, respectively. The vertical dashed black line indicated the peak of E7 wave storm.~~.~~

Con formato: Superíndice

Con formato: Subíndice

Con formato: Subíndice

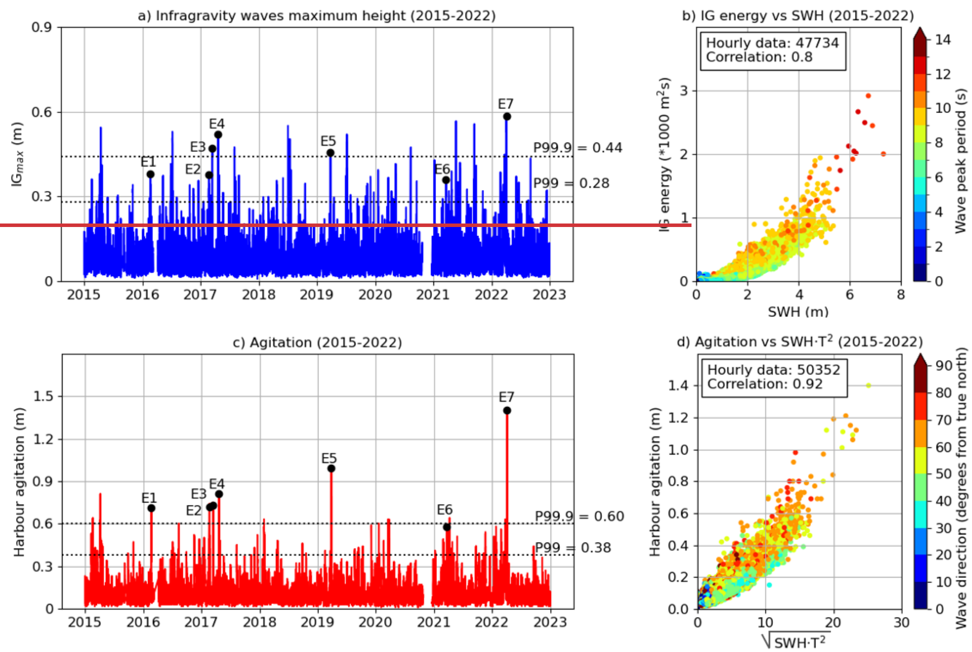
a) Infragravity waves maximum height (2015-2022)
IG$_{max}$ (m)
P99.9 = 0.44
P99 = 0.28
E1
E2
E3
E4
E5
E6
E7
b) IG energy vs SWH (2015-2022)
Hourly data: 47734
Correlation: 0.8
IG energy (*1000 m^{2}s)
SWH (m)
Wave peak period (s)
c) Agitation (2015-2022)
Harbour agitation (m)
P99.9 = 0.60
P99 = 0.38
d) Agitation vs SWH·T^2 (2015-2022)
Hourly data: 50352
Correlation: 0.92
$\sqrt{\text{SWH}\cdot\text{T}^2}$
Wave direction (degrees from true north)

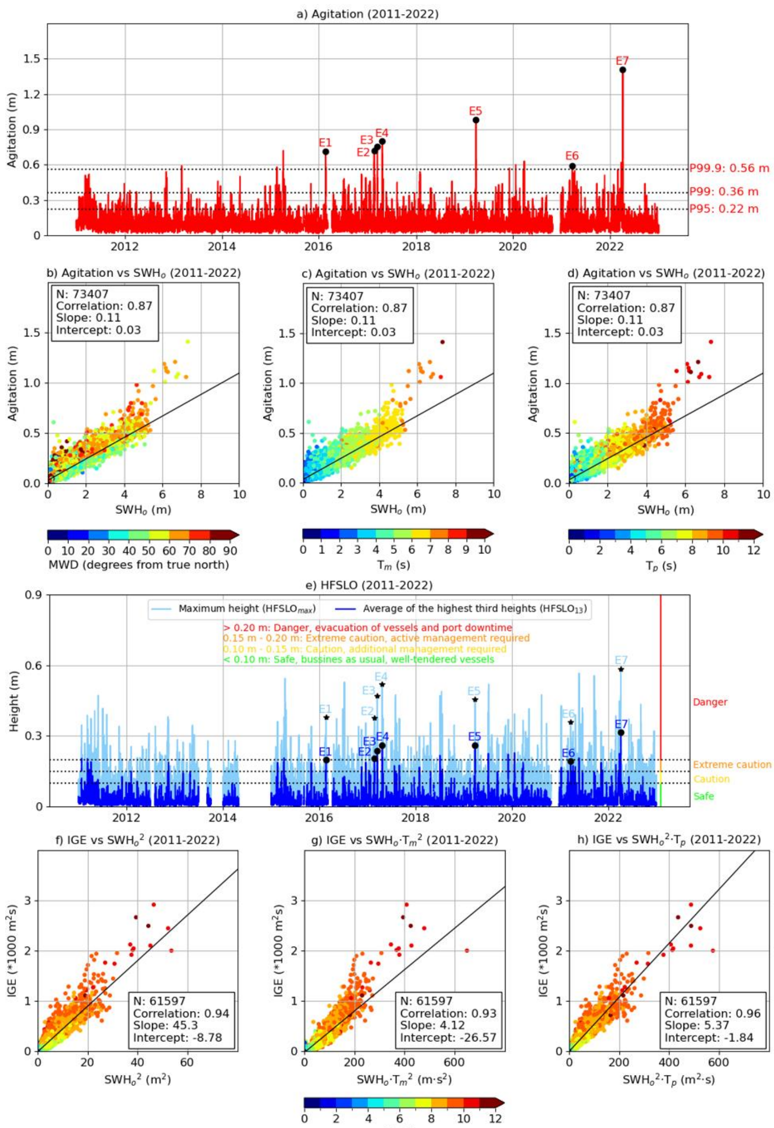
a) Agitation (2011-2022)
Agitation (m)
E1
E2
E3
E4
E5
E6
E7
P99.9: 0.56 m
P99: 0.36 m
P95: 0.22 m
b) Agitation vs SWHo (2011-2022)
c) Agitation vs SWHo (2011-2022)
d) Agitation vs SWHo (2011-2022)
N: 73407
Correlation: 0.87
Slope: 0.11
Intercept: 0.03
SWHo (m)
MWD (degrees from true north)
Tm (s)
Tp (s)
e) HFSLO (2011-2022)
Maximum height (HFSLOmax)
Average of the highest third heights (HFSLO13)
> 0.20 m: Danger, evacuation of vessels and port downtime
0.15 m - 0.20 m: Extreme caution, active management required
0.10 m - 0.15 m: Caution, additional management required
< 0.10 m: Safe, bussines as usual, well-tendered vessels
Height (m)
Danger
Extreme caution
Caution
Safe
f) IGE vs SWHo2 (2011-2022)
g) IGE vs SWHo·Tm2 (2011-2022)
h) IGE vs SWHo2·Tp (2011-2022)
IGE (*1000 m2s)
N: 61597
Correlation: 0.94
Slope: 45.3
Intercept: -8.78
Correlation: 0.93
Slope: 4.12
Intercept: -26.57
Correlation: 0.96
Slope: 5.37
Intercept: -1.84
SWHo2 (m2)
SWHo·Tm2 (m·s2)
SWHo2·Tp (m2·s)
Tp (s)

Figure 3. a) Hourly time series of agitation inside the harbour for the period 2011-2022 (product ref. no. 2 in Table 1) as provided by Melilla tide-gauge; b-d) Best linear fit (solid black line) of scatter plots of the harbour agitation against SWH, observations provided by Melilla coastal buoy. Statistical metrics are adhered in the white box, where N represents the number of hourly observations; ea) Hourly time series of High Frequency Sea Level Oscillations infragravity (IGHFSLO) ,with periods between 30 s and 1 h: maximum height wave maximum height (cyan line) and average of the highest third heights (blue line) for the period 20152011-2022 (product ref. no. 23 in Table 1), as registered by Melilla tide gauge (Figure 1, a-b). The seven extreme events analysed in this work are denoted by black stars and dots.; Thresholds for port management, which are universally common to all locations (McComb et al., 2020; McComb, 2011) are indicated with horizontal dotted lines; f-h)b) Best linear fit (solid black line) of sScatter plots of the energy in the IG band (IGE) against offshore hourly wave observations from Melilla coastal coastal buoy. (SWH and peak period); c) Hourly timeseries of agitation inside the harbour for the period 2015-2022 (product ref. no. 3 in Table 1); d) Scatter plot of the harbour agitation against the wave conditions outside the harbour (SWH and wave direction).

Con formato: Subíndice

Con formato: Fuente: Negrita

Con formato: Fuente: Negrita

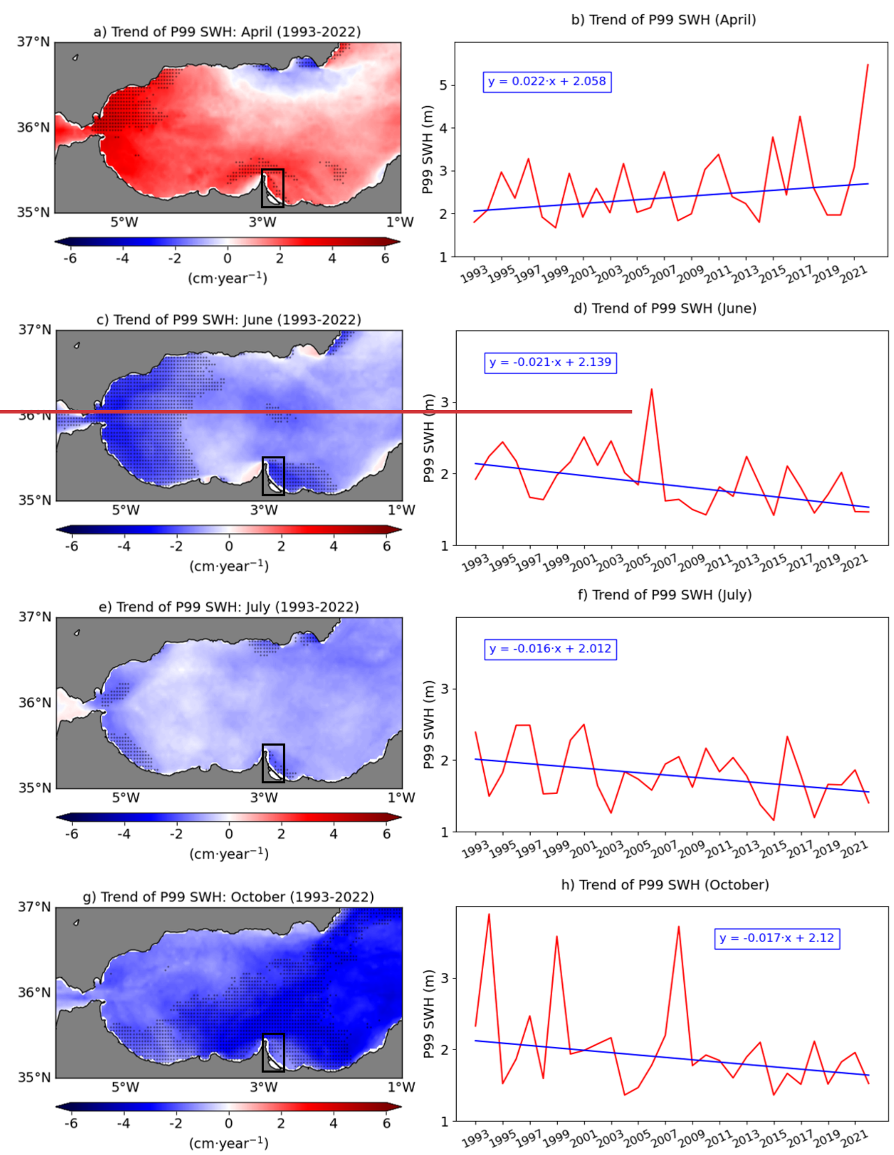
a) Trend of P99 SWH: April (1993-2022)
b) Trend of P99 SWH (April)
y = 0.022·x + 2.058
c) Trend of P99 SWH: June (1993-2022)
d) Trend of P99 SWH (June)
y = -0.021·x + 2.139
e) Trend of P99 SWH: July (1993-2022)
f) Trend of P99 SWH (July)
y = -0.016·x + 2.012
g) Trend of P99 SWH: October (1993-2022)
h) Trend of P99 SWH (October)
y = -0.017·x + 2.12
37°N
36°N
35°N
5°W
3°W
1°W
-6
-4
-2
0
2
4
6
(cm·year⁻¹)
P99 SWH (m)
1993
1995
1997
1999
2001
2003
2005
2007
2009
2011
2013
2015
2017
2019
2021

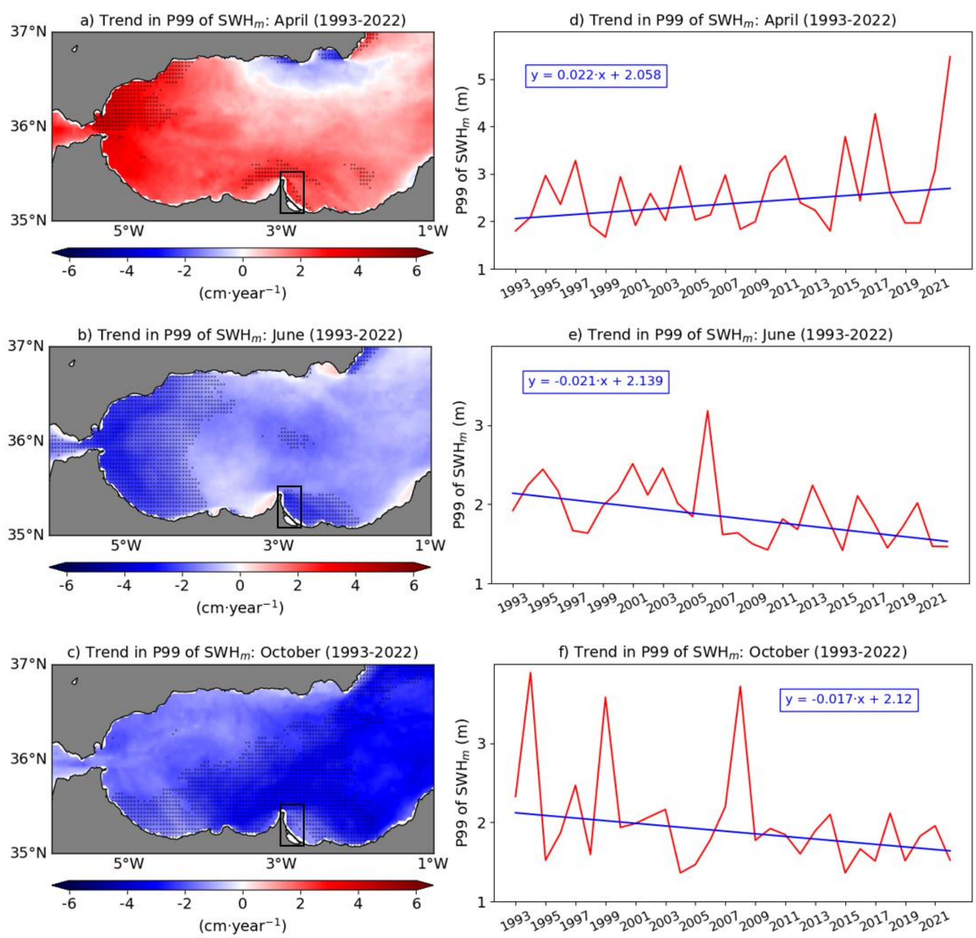

Figure 4. Left column: monthly trend maps of the 99th percentile (P99) of significant wave height (SWH$_m$) over the Alborán Sea for the 1993-2022 period as derived from ~~a regional~~ MED~~wave~~ reanalysis -product ref. no. 4~~5~~ (Table 1)-. Areas with statistically significant trends at the 90% confidence intervals are denoted by black dots. Right column: temporal trends, computed over the Melilla subdomain (represented by a black box in the associated maps).

Con formato: Superíndice

Con formato: Subíndice

Annex

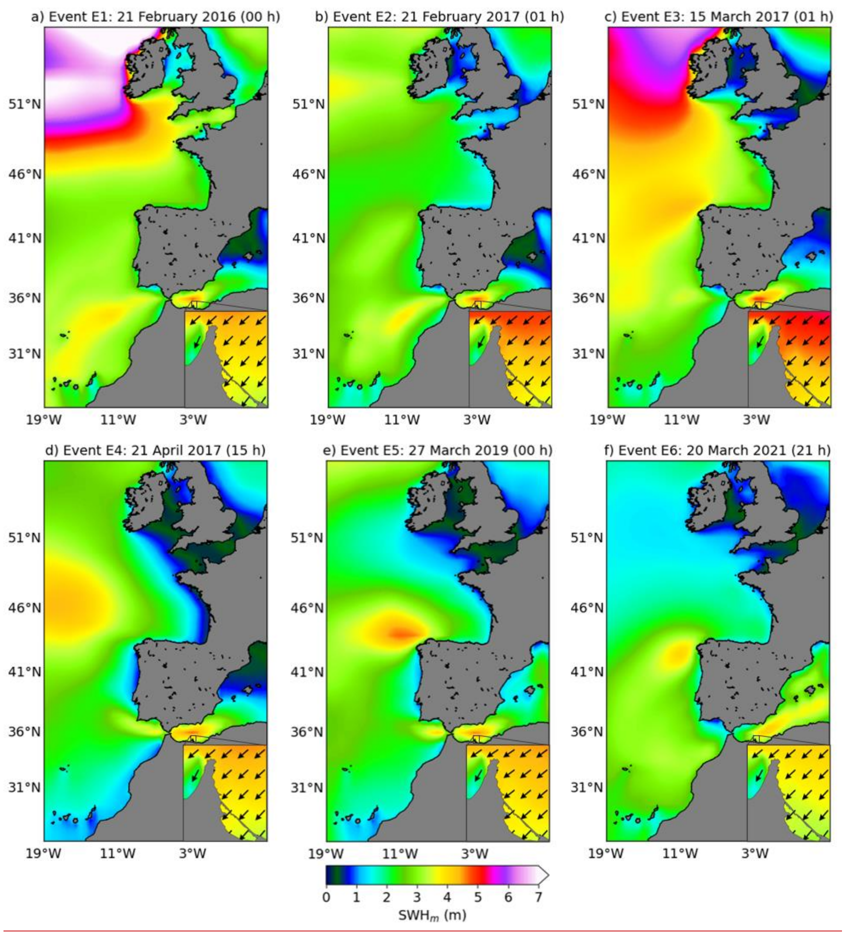

Annex 1. Hourly maps of significant wave height (SWH_m), derived from ERA5 reanalysis -product ref. no. 3 (Table 1)-, corresponding to six extreme wave events (E1-E6) affecting Melilla area. Small maps in the right bottom corner of each panel represent the hourly SWH_m and wave propagation direction in the vicinity of Melilla harbour as derived from MED reanalysis -product ref. no. 4 (Table 1)-. The hour represents local time.

Con formato: Normal

Con formato: Subíndice

Con formato: Subíndice

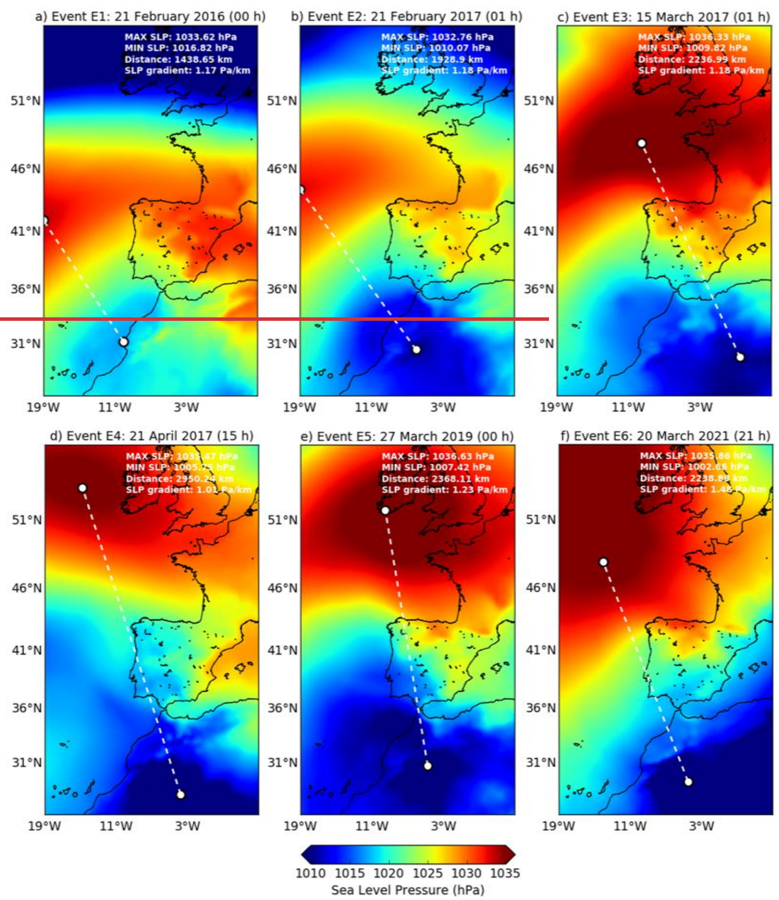
a) Event E1: 21 February 2016 (00 h)
MAX SLP: 1033.62 hPa
MIN SLP: 1016.82 hPa
Distance: 1438.65 km
SLP gradient: 1.17 Pa/km
b) Event E2: 21 February 2017 (01 h)
MAX SLP: 1032.76 hPa
MIN SLP: 1010.07 hPa
Distance: 1928.9 km
SLP gradient: 1.18 Pa/km
c) Event E3: 15 March 2017 (01 h)
MAX SLP: 1036.33 hPa
MIN SLP: 1009.82 hPa
Distance: 2236.99 km
SLP gradient: 1.18 Pa/km
d) Event E4: 21 April 2017 (15 h)
MAX SLP: 1035.47 hPa
MIN SLP: 1005.75 hPa
Distance: 2950.24 km
SLP gradient: 1.01 Pa/km
e) Event E5: 27 March 2019 (00 h)
MAX SLP: 1036.63 hPa
MIN SLP: 1007.42 hPa
Distance: 2368.11 km
SLP gradient: 1.23 Pa/km
f) Event E6: 20 March 2021 (21 h)
MAX SLP: 1035.86 hPa
MIN SLP: 1002.66 hPa
Distance: 2238.88 km
SLP gradient: 1.48 Pa/km
51°N
46°N
41°N
36°N
31°N
19°W
11°W
3°W
1010
1015
1020
1025
1030
1035
Sea Level Pressure (hPa)

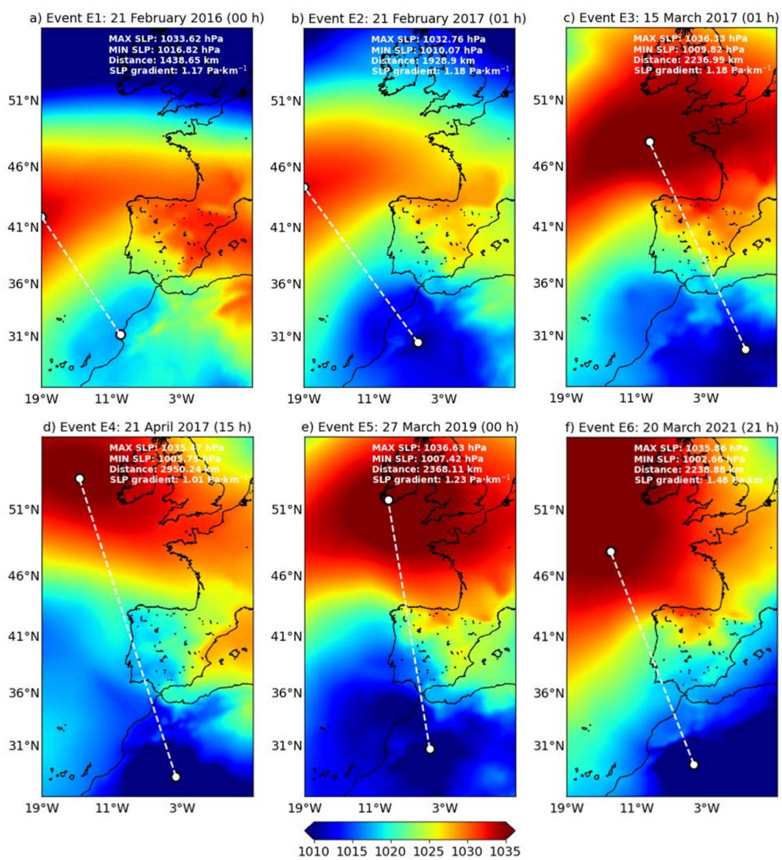

Annex 12. Hourly synoptic mapspatterns of sea level pressure (SLP), derived from ERA5 reanalysis -product ref. no. 3 (Table 1)-, corresponding to six extreme wave events (E1-E6) affecting Melilla area. corresponding to the 6 extreme wave events detected before the study case and listed in Figure 1d. Maps derived from ERA5 reanalysis -product ref. no. 1 (Table 1) . Maximum and minimum values of SPLP are marked with white dots and linked with a dashed white line. The distance between both andpressure centres and the related the SLP gradient areis indicated in the lower upper right corner. The hour represents local time.

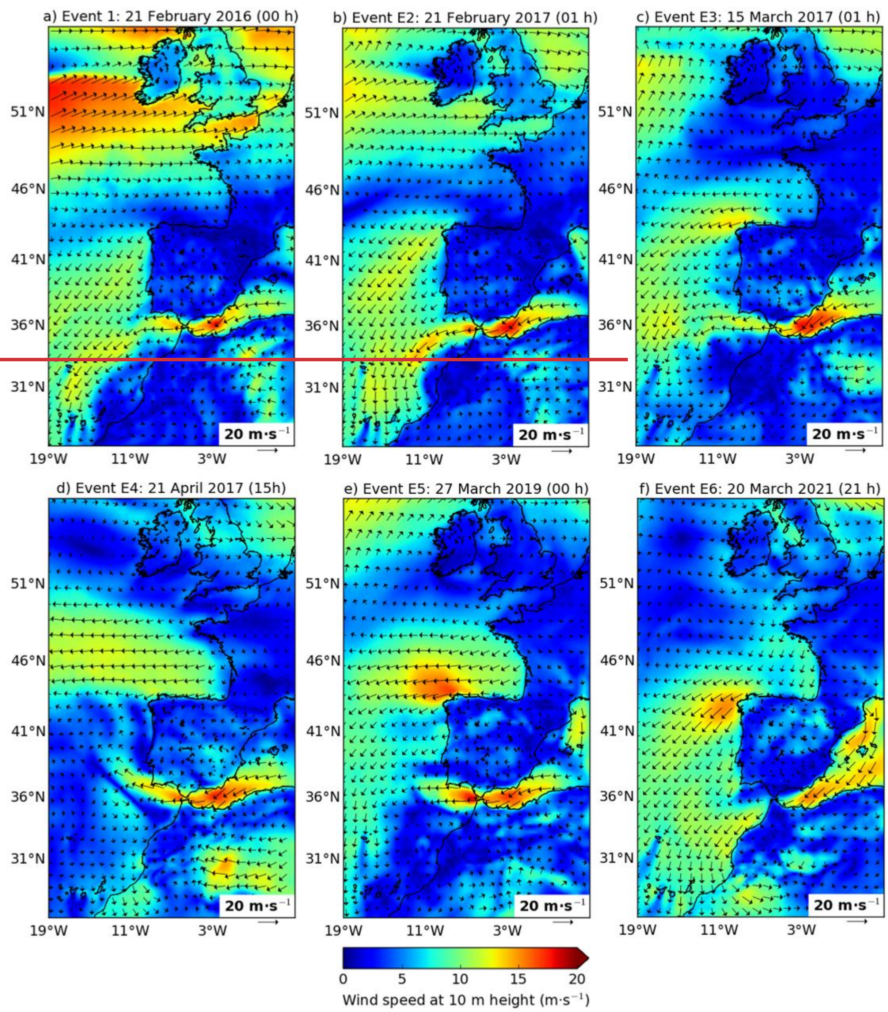
a) Event 1: 21 February 2016 (00 h)
b) Event E2: 21 February 2017 (01 h)
c) Event E3: 15 March 2017 (01 h)
d) Event E4: 21 April 2017 (15h)
e) Event E5: 27 March 2019 (00 h)
f) Event E6: 20 March 2021 (21 h)
51°N
46°N
41°N
36°N
31°N
19°W
11°W
3°W
20 m·s⁻¹
0
5
10
15
20
Wind speed at 10 m height (m·s⁻¹)

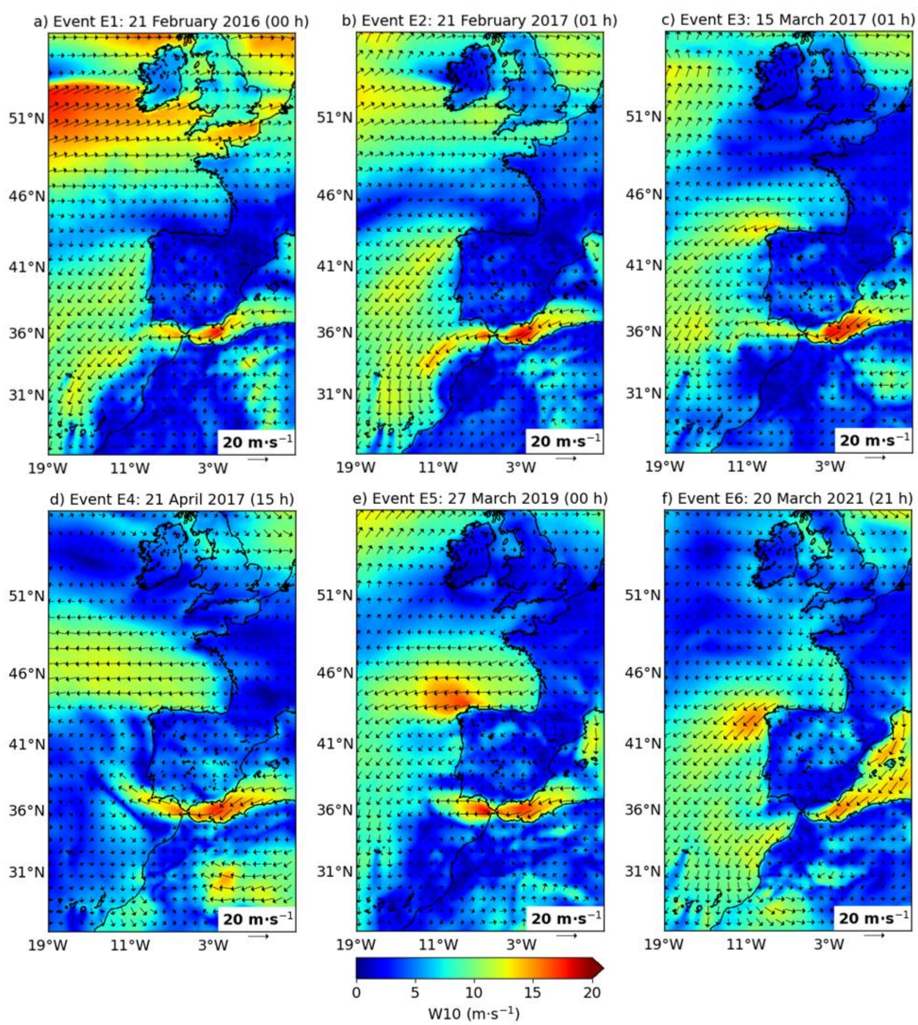

Annex 23. Hourly synoptic mapspatterns of wind at 10 m height (W10), derived from ERA5 reanalysis -product ref. no. 3 (Table 1)-, corresponding to six extreme wave events (E1-E6) affecting Melilla area. corresponding to the 6

extreme wave events detected before the study case and listed in Figure 1d. Maps derived from ERA5 reanalysis - product ref. no. 1 (Table 1) .The hour represents local time.

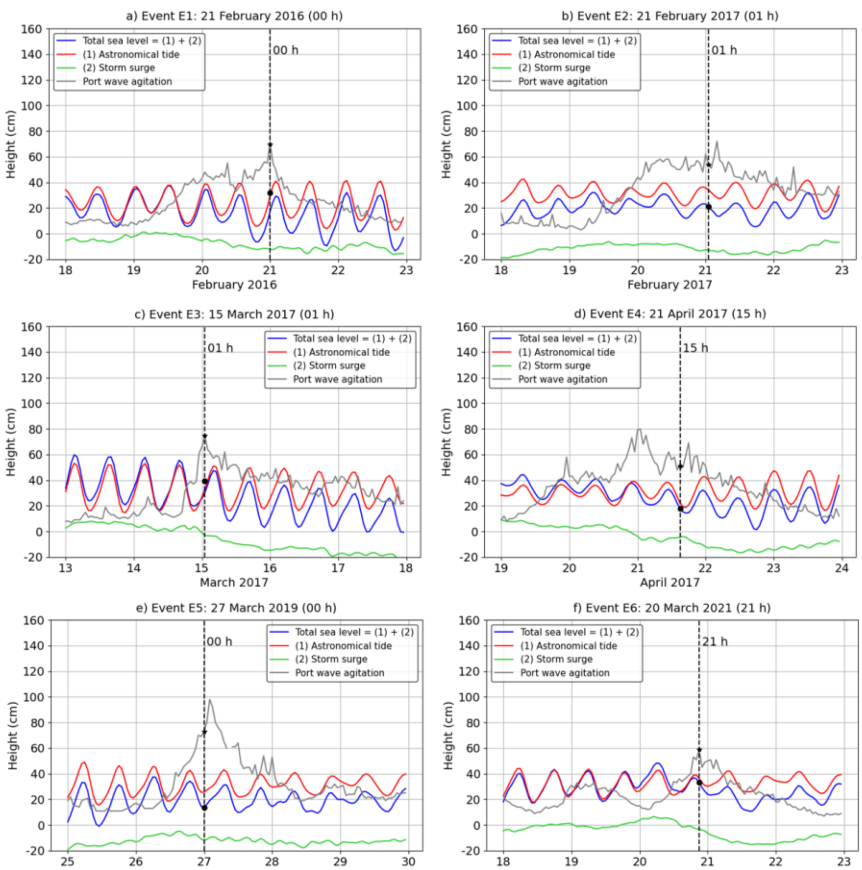

Annex 4. Hourly times series of sea level height (blue line) and port agitation (grey line) observations corresponding to the six extreme wave events detected before the study case and labelled in Figure 1d. Observations provided by Melilla tide-gauge (product ref. no. 2 in Table 1). Astronomical tides and meteorological residuals are represented by

the red and green lines, respectively. The vertical dashed black line indicated the peak of the wave storm for each of the six events analysed.

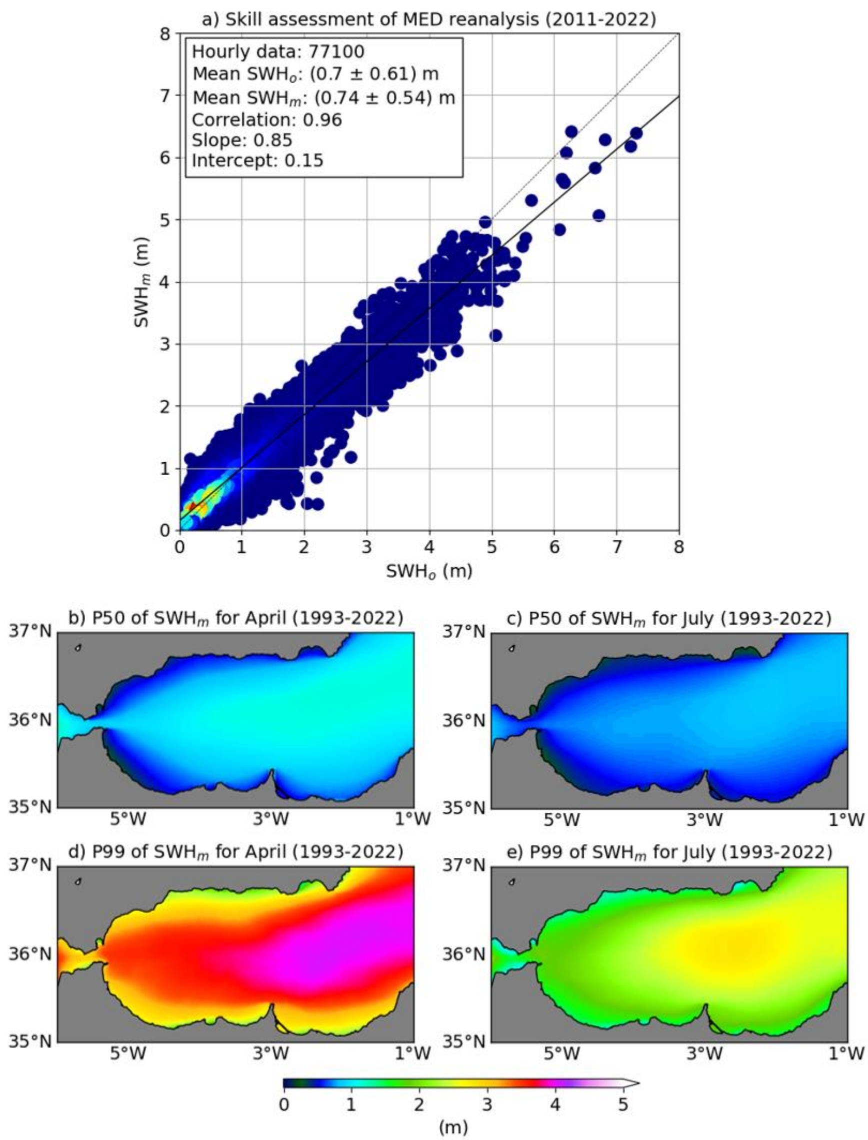
a) Skill assessment of MED reanalysis (2011-2022)
Hourly data: 77100
Mean SWH_o: (0.7 ± 0.61) m
Mean SWH_m: (0.74 ± 0.54) m
Correlation: 0.96
Slope: 0.85
Intercept: 0.15
SWH_m (m)
SWH_o (m)
b) P50 of SWH_m for April (1993-2022)
c) P50 of SWH_m for July (1993-2022)
d) P99 of SWH_m for April (1993-2022)
e) P99 of SWH_m for July (1993-2022)
37°N
36°N
35°N
5°W
3°W
1°W
(m)

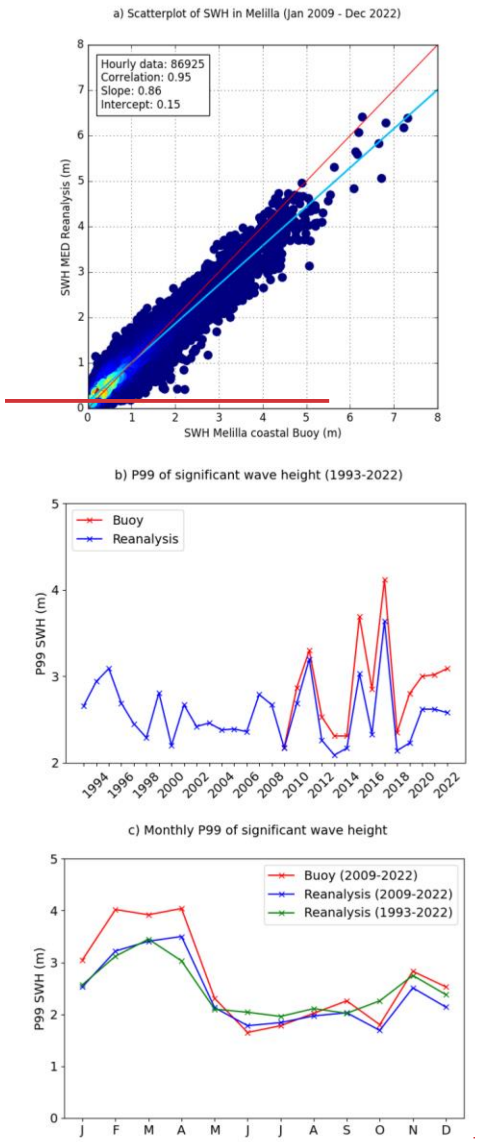

Con formato: Justificado

Annex 53. a) a) Skill assessment of the regional MEDwave reanalysis -product ref. no. 45 (Table 1)- at the grid point closest to against Melilla coastal buoy -product ref. no. 14 (Table 1)-: best linear fit (solid black line) of scatter plot between hourly estimations of modelled (SWH_m) and observed (SWH_o) significant wave heigh in situ observations of significant wave height (SWH) and modelled outputs in the grid point closest to the moored buoy for athe concurrent 1214-year period (20201109-2022). The dotted black, line represents the result of perfect agreement with slope 1.0 and intercept 0. Statistical metrics are adhered in the white box; b) Spatial distribution of the 50th -P50- (b, c) and 99th -P99- (d, e) percentiles of SWH_m over the Alborán Sea for April (b, d) and July (c , e), as derived from MED reanalysis for the 1993-2022 period.; b) Annual values of observed (red line) and modelled (blue line) P99 of SWH in Melilla; c) Monthly values of observed (red line: 2009-2022) and modelled (blue line for 2009-2022, green line for 1993-2022) P99 of SWH in Melilla.

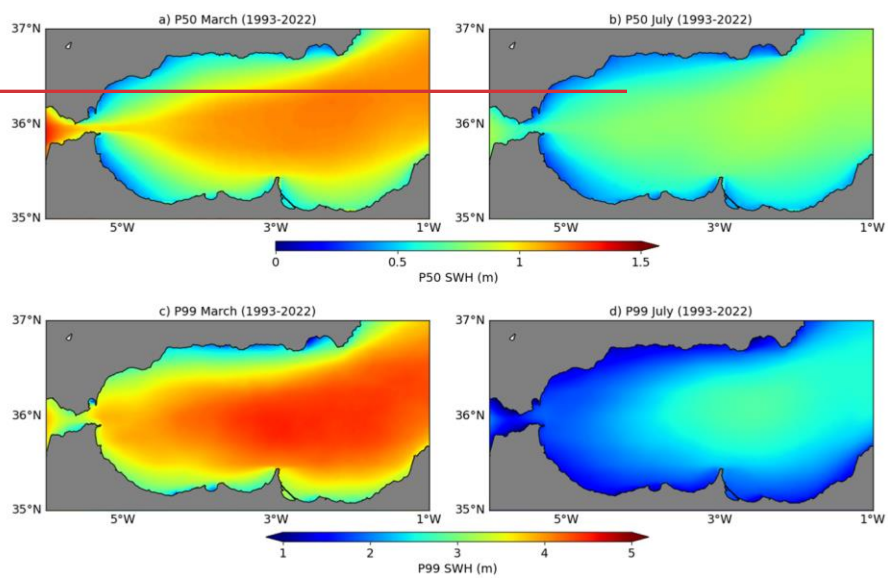

Annex 4. Spatial distribution of the 50th -P50- (a-b) and 99th -P99- (c-d) percentiles of significant wave height (SWH) over the Alborán Sea for January (left column) and July (right column), as derived from the regional wave reanalysis product for the 1993-2022 period -product ref. no. 5 (Table 1)-.

Con formato: Subíndice

Con formato: Fuente: Negrita

Con formato: Superíndice

Con formato: Superíndice

Con formato: Subíndice

1125

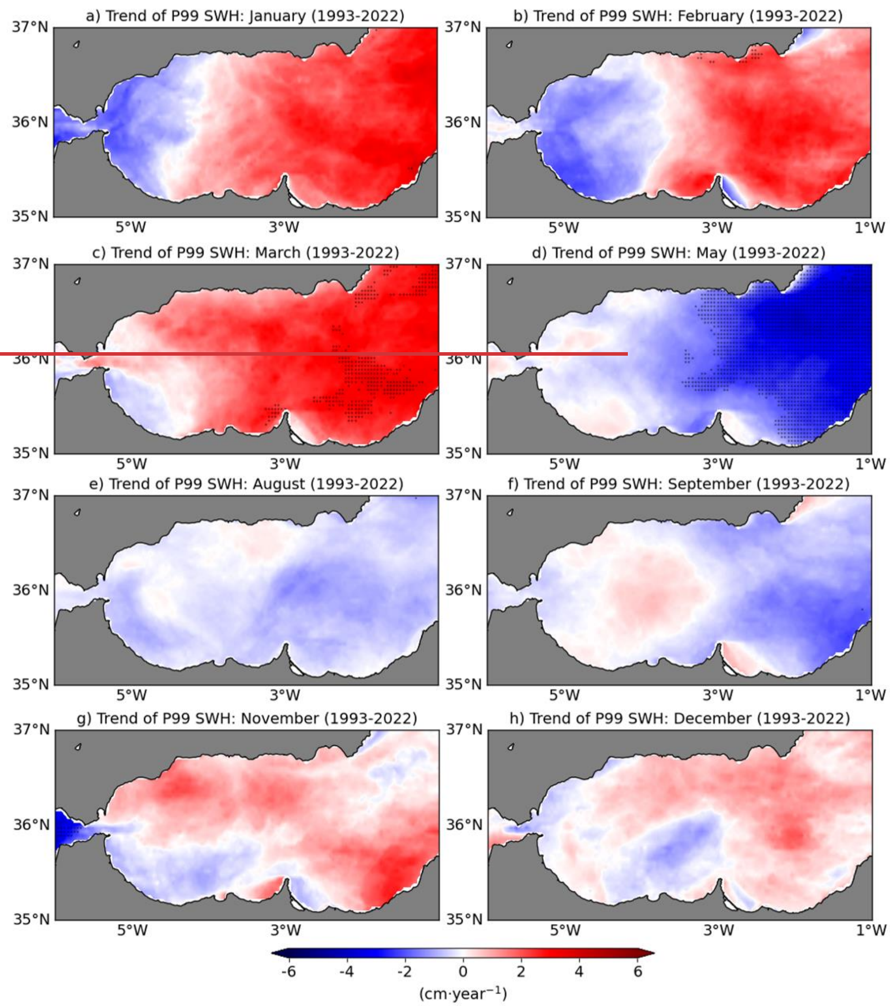

~~**Annex 5. Trends of the 99th percentile (P99) of significant wave height (SWH) over the Alborán Sea for the 1993-2022 period as derived from the regional wave reanalysis product ref. no. 5 (Table 1). Areas with statistically significant trends at the 90% confidence intervals are denoted by black dots.**~~

1135